Monthly Notices
of the
ROYAL ASTRONOMICAL SOCIETY

MNRAS **461,** 3089–3110 (2016)
Advance Access publication 2016 June 24

doi:10.1093/mnras/stw1534

Linear spectropolarimetry across the optical spectrum of Herbig Ae/Be stars⋆

K. M. Ababakr,[1]† R. D. Oudmaijer[1] and J. S. Vink[2]

[1]*School of Physics and Astronomy, University of Leeds, EC Stoner Building, Leeds LS2 9JT, UK*
[2]*Armagh Observatory, College Hill, Armagh, UK*

Accepted 2016 June 22. Received 2016 June 22; in original form 2016 April 29

ABSTRACT

We present the results of spectropolarimetric observations of 12 Herbig Ae/Be objects. Our data have the largest spectropolarimetric wavelength coverage, 4560–9480 Å, published to date. A change in linear polarization across the H α line, is detected in all objects. Such a line effect reveals the fact that stellar photons are scattered off free electrons that are not distributed in a spherically symmetric volume, suggesting the presence of small discs around these accreting objects. Thanks to the large wavelength coverage, we can report that H α is the spectral line in the optical wavelength range that is most sensitive to revealing deviations from spherical symmetry, and the one most likely to show a line effect across the polarization in such cases. Few other spectral lines display changes in polarization across the line. In addition, H α is the only line which shows an effect across its absorption component in some sources. We present a scenario explaining this finding and demonstrate that the detection of the line effect strongly relies on the number of photons scattered into our line of sight. We highlight the special case of R Mon, which is the only object in our sample to show many lines with a polarization effect, which is much stronger than in all other objects. Given that the object and its nebulosity is spatially resolved, we argue that this is due to scattering of the stellar and emission spectrum off circumstellar dust.

Key words: techniques: polarimetric – circumstellar matter – stars: formation – stars: individual: Herbig Ae/Be – stars: pre-main-sequence.

1 INTRODUCTION

Despite the important role of massive stars in the evolution of the interstellar medium and unlike their counterpart low-mass stars that are thought to be formed via magnetospheric accretion (Muzerolle, Calvet & Hartmann 1998), their accretion mechanism is still open to debate. Observationally, the detection of massive stars is challenging as they reside far away and are deeply embedded in their natal clouds. As an alternative to massive stars, the intermediate mass Herbig Ae/Be (HAeBe) stars are the best candidates to address this issue. They are optically visible and bridge the gap between low- and high-mass stars. They were first identified by Herbig as having a spectral type A or B with emission lines (Herbig 1960). The current view is that HAeBe stars are surrounded by discs through which material continues to accrete on to the star (e.g. Ilee et al. 2014), although the precise scenario is not known (for reviews on the topic, see Grady et al. 2015; Kraus 2015; Beltrán & de Wit 2016).

In order to make progress, one needs to study the circumstellar environment through which the material accumulates on to the star via accretion channels. This requires methods capable of probing the matter very close to the star, as this is where the accretion action happens. A key point is the observation whether the ionized region around the star is spherically symmetric at small scales or not. If it is not, then the possibility that a flattened structure is observed lends support to the disc accretion scenario responsible for the formation of such stars. Studying the circumstellar environment at these small scales is possible through linear spectropolarimetry, measuring the scattering of photons off free electrons in a dense, ionized gas.

The idea of spectropolarimetry is that in the ionized region, free electrons scatter and polarize continuum photons from the central star. If the geometry is not circular on the sky, for example in the case of flattened disc, a net polarization can be detected. However, emission photons undergo less scattering as they emerge further away from the central star. If we are to measure the polarization as a function of wavelength, this difference in scattering will be visible as a change in polarization across the line, which is often simply referred to as the 'line effect'. The observed depolarization

⋆ Based on observations collected at the European Southern Observatory (ESO), Paranal, Chile under programme 088.C-0858(A), 088.C-0858(B) and 088.C-0858(C).

† E-mail: pykma@leeds.ac.uk

Table 1. HAeBe Observations. The *V* magnitude and spectral type are listed in columns 3 and 4. The spectral type is taken from Ababakr et al. (2015) and Fairlamb et al. (2015) while the *V* magnitude is taken from Vieira et al. (2003) and SIMBAD. The integration times (columns 8–10) denote the total exposures in *V* (4560–5860 Å), *R* (5750–7310 Å) and *Z* (7730–9480 Å) bands.

Name	Other name	*V*	Spec. type	Date			Exposure (s)		
				V	*R*	*Z*	*V*	*R*	*Z*
PDS 27	DW CMa	13.0	B3	04-02-12	04-02-12	04-02-12	8 × 340	24 × 50	16 × 120
PDS 37	Hen 3-373	13.5	B3	05-02-12	05-02-12	05-02-12	16 × 340	24 × 70	16 × 100
CPD-485215	Hen 3-847	10.6	B6	20-01-12	10-03-12	03-03-12	8 × 150	32 × 15	16 × 90
R Mon	MWC 151	11.8	B8	19-02-12	01-02-12	01-02-12	4 × 340	12 × 85	12 × 80
					12-10-11			12 × 85	
V380 Ori	–	10.7	A0	03-01-12	03-01-12	10-11-11	8 × 60	16 × 20	12 × 20
					12-10-11			12 × 20	
PDS 133	SPH 6	13.1	B6	–	21-01-12	21-01-12	–	16 × 150	8 × 340
BF Ori	–	9.7	A2	–	12-10-11	12-11-11	–	8 × 75	8 × 90
MWC 275	HD 163296	6.9	A1	–	01-04-12	30-03-12	–	32 × 2.5	16 × 7.5
GU CMa	HD 52721	6.6	B1	–	07-01-12	07-01-12	–	24 × 2	24 × 5
HD 104237	PDS 61	6.6	A7	–	16-01-12	16-01-12	–	40 × 1	24 × 5
HD 85567	–	8.6	B7	–	30-12-11	08-12-11	–	8 × 5	16 × 30
					30-03-12			8 × 5	
HD 98922	Hen 3-644	6.8	A0	–	30-12-11	16-01-12	–	40 × 1.5,16 × 1	24 × 5

across the H α line constituted the first evidence that the class of Be stars were surrounded by discs (Clarke & McLean 1974; Poeckert & Marlborough 1976). This was only much later confirmed by direct observations (e.g. Quirrenbach et al. 1994, based on image reconstruction of interferometric data; Wheelwright et al. 2012, using sub-milliarcsecond precision spectro-astrometry).

Oudmaijer & Drew (1999), Vink et al. (2002) and Mottram et al. (2007) extended the use of the technique to HAeBe objects. Vink et al. (2002) found that 7 out of 12 Herbig Be (HBe) objects they observed have a depolarization line effect across H α, very similar to what was found in Be stars. As the line effect becomes less pronounced for lower inclinations, and would disappear for a face-on disc, which is circular on the sky, the detection statistic strongly suggests that all HBe stars are surrounded by small discs with sizes of order several stellar radii. In contrast, they found a different line effect for Herbig Ae (HAe) objects, where enhanced *polarization* across the H α was found in 9 out of 11 stars. They proposed that the line itself is intrinsically polarized since part of the emission lines originate from a compact region, where the accretion takes place. Vink et al. (2005) found that HAe stars have a similar spectropolarimetric signature as the lower mass T Tauri stars with HBe stars having a different signature.

McLean (1979) reported a different line effect, across the absorption component of the emission line which is often called the McLean effect. The general idea is that the absorption blocks the unscattered light from the beam, and photons originally emitted in different directions are scattered into the line of sight, resulting in enhanced polarization across the absorption. An alternate hypothesis was provided by Kuhn et al. (2007), who proposed the polarization can be caused by selective absorption due to optical pumping of an anisotropic radiation field. In addition, Kuhn, Geiss & Harrington (2011) point out that resonant line scattering, which potentially also produces line polarization, predicts that the lines within the Ca II near-infrared triplet around 8500 Å will be differently polarized from each other. For a recent review on the use of linear spectropolarimetry, see Vink (2015).

In this work, we aim to expand the existing spectropolarimetric work that was mostly aimed at H α by observing other emission lines probing different volumes and conditions than H α. Here we present a spectropolarimetric study of a sample of 12 HAeBe objects. The new feature of the current study is the broad wavelength range from 4560 to 9480 Å, covering almost the entire optical spectrum. The paper is organized as follows. In Section 2, we discuss the sample selection criteria, the details of the observations and data reduction. In Section 3, we present the results starting with continuum polarization and then discussing line spectropolarimetry. The analysis is provided in Section 4. We conclude in Section 5.

2 OBSERVATIONS

2.1 Source selection

12 objects were selected for this work from the X-shooter project of 91 HAeBe stars (Oudmaijer et al. 2011; Fairlamb et al. 2015). The main reason for choosing these, was the presence of strong emission lines which allows for a good determination of their spectropolarimetric properties. The targets were originally selected from the HAeBe catalogue of The, de Winter & Perez (1994) and candidates of Vieira et al. (2003). They are presented in Table 1, alongside their spectral type and *V* magnitudes. The spectral type is taken from Ababakr et al. (2015) and Fairlamb et al. (2015) while the *V* magnitude is taken from Vieira et al. (2003) and SIMBAD. The results of PDS 27 and PDS 37 have been published elsewhere in a study dedicated to these two objects, but we keep them in here (Ababakr et al. 2015).

2.2 Spectropolarimetric observations

The spectropolarimetric data were obtained with the FORS2 spectrograph mounted on ESO's VLT in Chile. The 1400V, 1200R and 1027Z gratings centred at 5200 Å, 6500 Å and 8600 Å, respectively were used with a 4096 × 2048 pixel CCD to cover the entire optical range from 4560 to 9480 Å. A spectral resolution of $R = 3800$, 4800, 4800 was achieved in the *V*, *R*, and *Z* bands, respectively, using the 0.5 arcsec slit. The dates and the exposure times for each band are given in Table 1.

The optical polarimeter in FORS2 was employed for the linear polarization observations. It consists of a rotating half-wave plate and a calcite block. The half-wave plate can be set to various angles to get *QU* Stokes parameters while the calcite block separates the

light into two perpendicularly polarized light beams, the ordinary (O) and extraordinary (E) beam. Four exposures with the half-wave plate set at angles 0°, 45°, 22.5°, and 67.5° provide a complete set of observations. At each angle, four spectra are obtained; the O and E beam of the object and sky respectively. Several cycles of observation at the above four angles were taken for each object to check for the consistency of the polarization and its features. Several polarized standard stars and unpolarised standard stars were observed to calibrate the instrumental polarization and angle offset.

Spectropolarimetry is a photon-hungry method. Typical line effects are of order 0.5 per cent and to properly sample the polarization behaviour as a function of wavelength, a polarization precision of order 0.1 per cent per pixel is therefore required. This corresponds to signal-to-noise ratios of order 1000. We used long exposure times for faint objects and several short exposure times for objects with strong H α lines in order to avoid saturation of the CCD.

2.3 Data reduction

The data reduction was carried out using GASGANO and FORS pipeline v4.9.18, which includes bias subtraction, flat fielding, sky subtraction, extraction and wavelength calibration of the O and E spectra. The Stokes parameters were determined from the O and E spectra. Finally, the percentage of linear polarization, P, and polarization angle, θ, were obtained according to the following equations:

$$P = \sqrt{Q^2 + U^2} \tag{1}$$

$$\theta = \frac{1}{2} \arctan\left(\frac{U}{Q}\right). \tag{2}$$

For the analysis purposes, the data were imported into the IRAF (Tody 1993) and POLMAP package (Harries 1996) maintained by Starlink. The individual data sets were combined to improve the quality of the data. Four polarized and three zero polarized standard stars were selected from the sample of Fossati et al. (2007) for polarimetric calibrations. The instrumental polarization is found to be ∼0.16 per cent, from the observation of unpolarized standard stars. The angle offset is found to be 0.5° from the observation of polarized standard stars. In order to clearly visualize the line effect, the change in polarization across the lines, we rebin the polarization spectra to a maximum polarization error per bin. We performed the rebinning of the spectra very carefully to avoid losing the line effect signature. We did not correct the data for the instrumental and interstellar polarization. These two parameters only add a, small, wavelength independent vector to the observed Q and U parameters whereas our main aim in this work is the detection of polarimetric change across the lines. However, as the polarization is a vector quantity, the interstellar polarization could change the appearance of the polarization signature across the line (see e.g. Oudmaijer et al. 1998 in HD 87643). Therefore, careful analysis is needed to characterize the line effect.

2.4 The optical spectrum

In the optical range from 4560 to 9480 Å, the spectra show numerous spectral lines in emission and absorption. The entire spectrum of PDS 27 is presented in Fig. 1 to show the range of the observed spectra and the identified spectral lines.

The H α lines are the strongest with line peak to continuum ratios ranging from ∼2 to ∼20. In all targets, H α is in emission, as shown in Fig. 2. The H α lines exhibit various different profiles. These

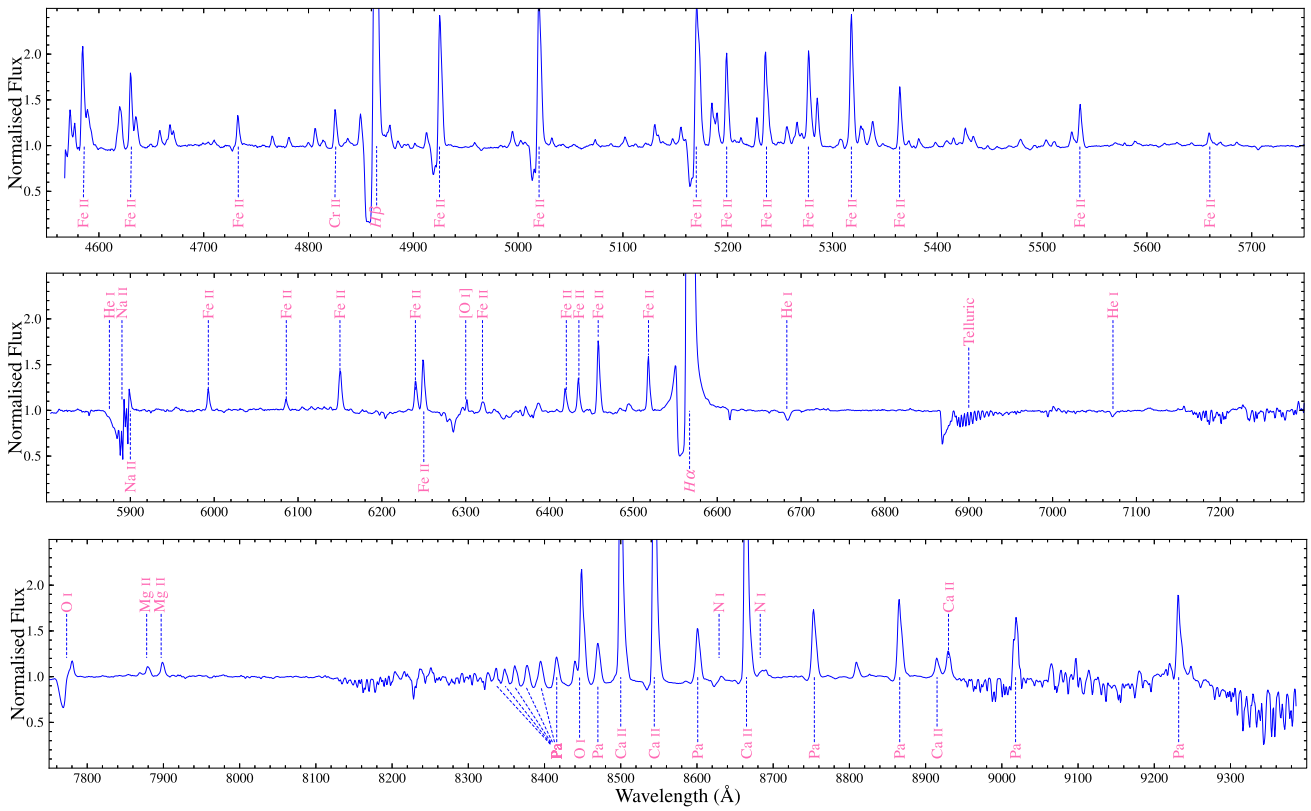

Figure 1. Normalized flux versus wavelength (Å) spectra of PDS 27 in the range from 4560 to 9480 Å, the observed spectral lines are identified.

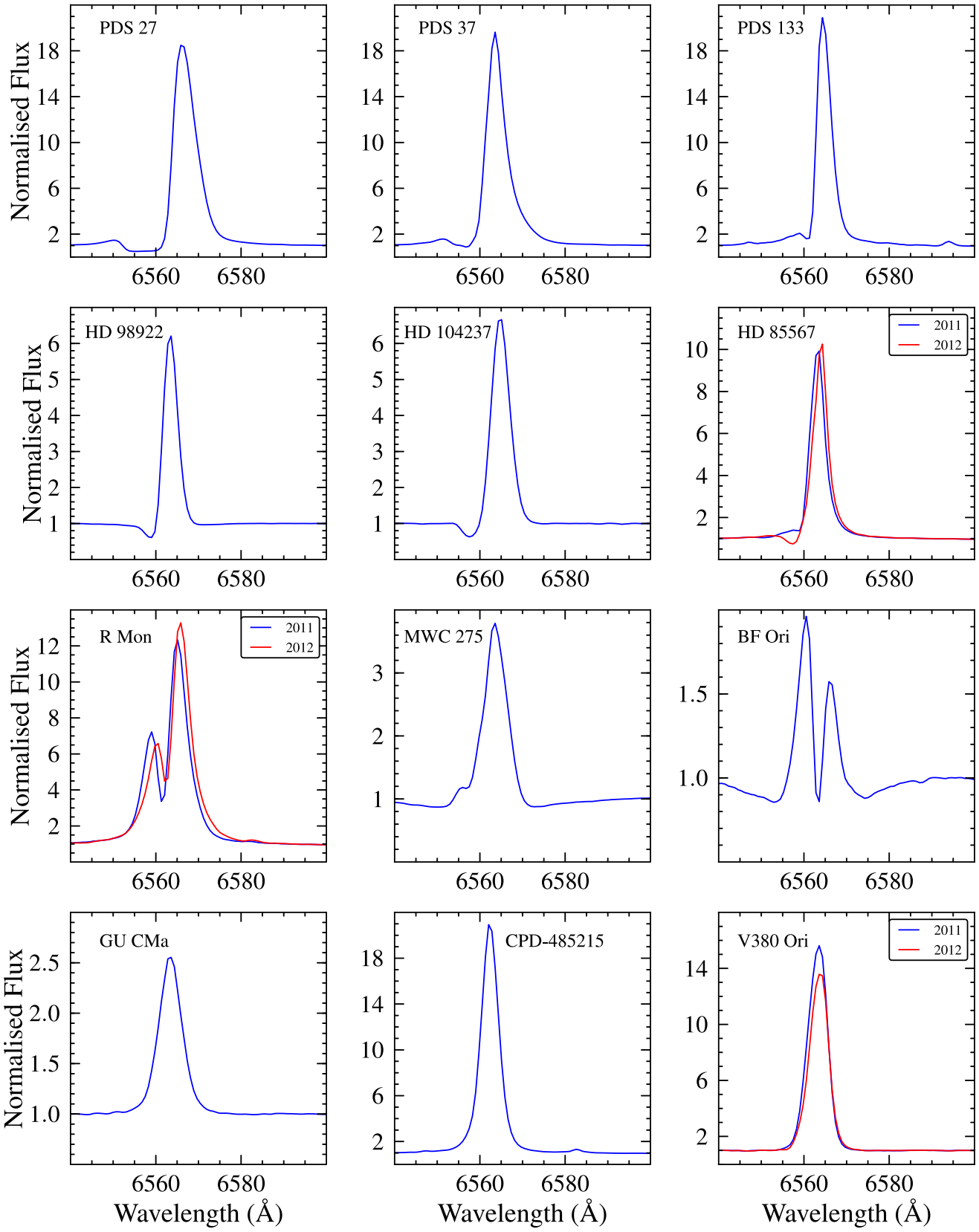

Figure 2. The H α line profiles, the spectra are normalized to one. The spectra of HD 85567, R Mon and V380 Ori are presented for two observation epochs: 2011 (blue solid line) and 2012 (blue solid line).

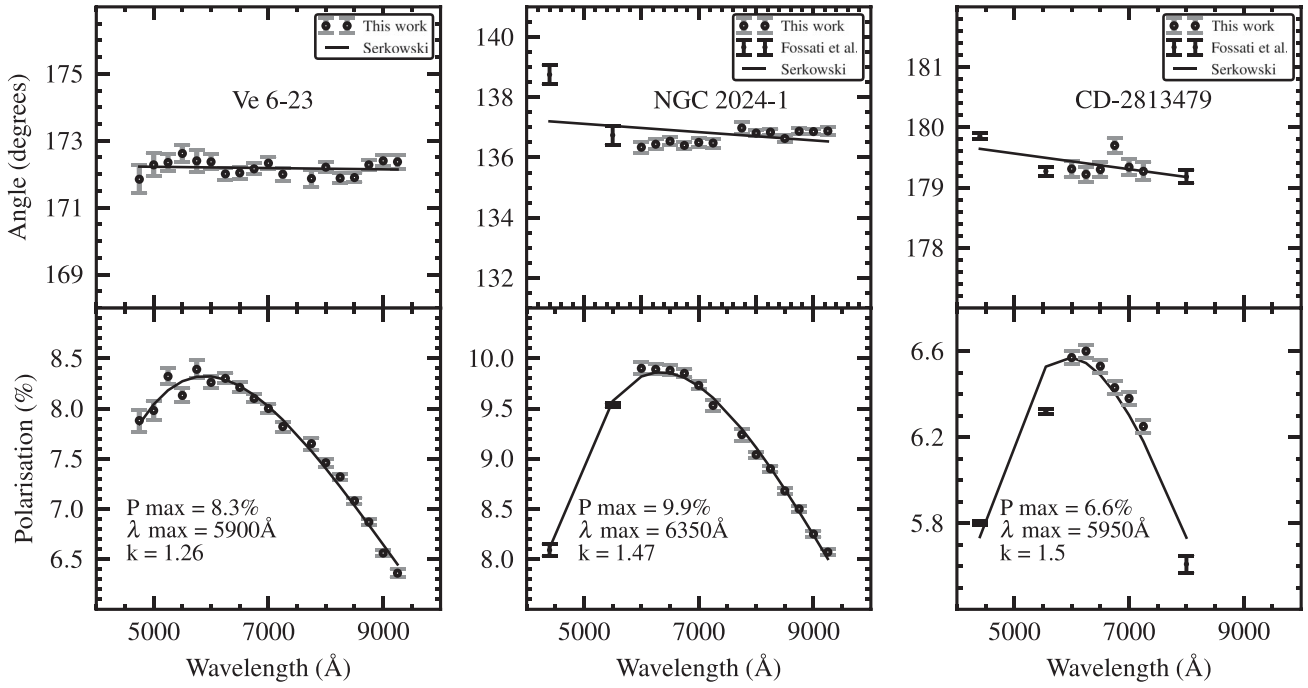

Figure 3. The polarization and polarization angles as a function of wavelength for the polarized standard stars. The data for this work are presented in black solid circles and were coarsely sampled to improve the error bars. The data in *B* and *V* for NGC 2024-1, and in *B*, *V* and *I* (black dots) are taken from Fossati et al. (2007). The black lines denote the best-fitting Serkowski law to the data.

include pure emission lines, double peaked emission with central absorption through to P Cygni profiles. GU CMa, CPD-485215 and V380 Ori display a pure emission line, R Mon and BF Ori show a double peaked emission line with central absorption. The remaining seven objects display P Cygni profiles, for two of which we also have H β data. For both spectra that contain H β, the absorption component in H β is deeper than in H α. In addition to Balmer series, weak Paschen lines are also seen in emission for most objects.

The Ca II triplet lines at 8498, 8542 and 8662 Å are observed in all objects apart from GU CMa and CPD-485215. They are all in emission apart from BF Ori where they are in absorption. The line to continuum ratio is in the range 1.5–10.5. The Ca II doublet at 8912 and 8927 Å is present in all objects apart from GU CMa, MWC 275 and CPD-485215. The lines are in emission in all objects apart from HD 104237 and BF Ori where the lines are in absorption.

Three He I lines at 5876, 6678 and 7065 Å are observed in all objects. The lines are in absorption in six objects including PDS 27, PDS 37, R Mon, HD 85567, GU CMa and BF Ori. PDS 133, HD 104237, V380 Ori and HD 98922 have the lines in emission. Inverse P Cygni profiles, weak emission and strong absorption He I lines are detected in the spectra of MWC 275 and CPD-485215 and indicate infalling material.

Several forbidden [Fe II] at 4814, 5158, 5262, 5333, 7155 and 8616 Å lines are observed in the spectra of R Mon and CPD-485215. [S II] at 6716 and 6730 Å is also seen in the spectra of R Mon. In addition, strong [O I] at 6300, 6364 Å is present in the spectra of R Mon, CPD-485215 and PDS 133. However, [O I] lines are either absent or very weak in the spectra of the remainder of the targets. Unlike the cases of R Mon and CPD-485215, the [O I] lines in the spectra of PDS 133 are broad and double peaked which may suggest that the forbidden lines emerge from a rotating disc. This has been suggested before for HAeBe stars (Acke, van den Ancker & Dullemond 2005), although the broad line could also indicate a disc-wind (see e.g. Ignace & Brimeyer 2006).

In summary, we observe many strong emission lines which allows us to investigate spectropolarimetric line effects which had never been done before studied for most of these lines.

3 RESULTS

3.1 Continuum polarization

The continuum polarization is measured for the entire spectrum and the results for the polarimetric standard stars are shown in Fig. 3, while those for the HAeBe stars are plotted in Fig. 4. The data are rebinned using a coarse sampling of ∼250 Å per bin, to minimize errors.

Typically, the observed continuum polarization is a vector addition of the interstellar polarization and the intrinsic polarization which is due to scattering of star light by circumstellar dust and free electrons. The interstellar polarization is caused by dichroic absorption of aligned dust grains. Its wavelength dependence is well understood and explained by Serkowski, Mathewson & Ford (1975). They found that the linear polarization follows an empirical curve according to the following equation:

$$\frac{P(\lambda)}{P_{\max}} = \exp\left[-k\ln^2\left(\frac{\lambda_{\max}}{\lambda}\right)\right], \quad (3)$$

where $\lambda_{\max}$ is the wavelength where the polarization is at its maximum value, $P_{\max}$, and k is the width of the empirical curve. Typically, the polarization peaks in the visual band at ∼5500 Å, but can be in the range of 4500–8000 Å. k was initially taken to be a constant value of $k = 1.15$. However, it has been found that the value of k depends on the value of $\lambda_{\max}$, and is sensitive to the size distribution

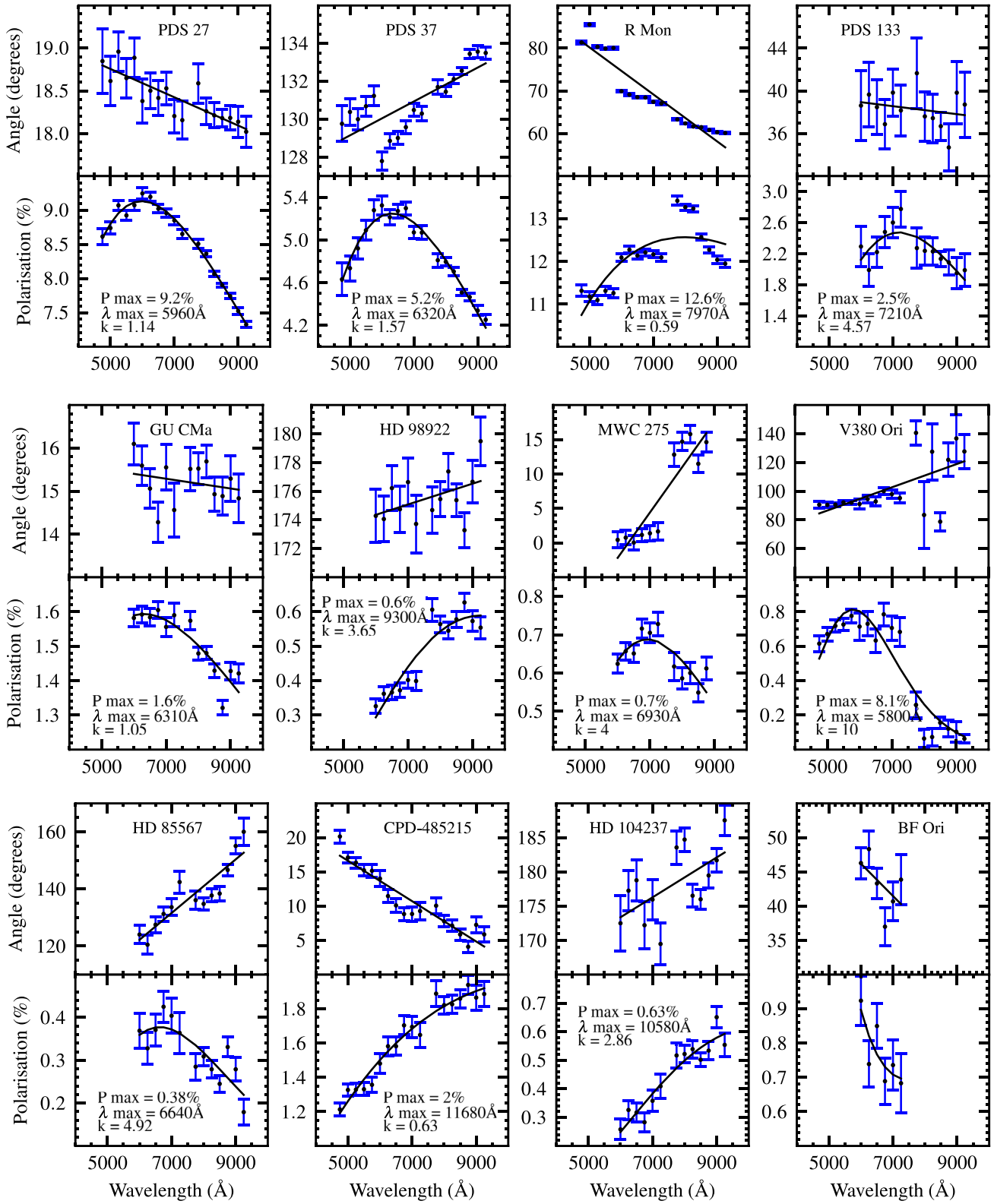

Figure 4. As the previous figure, but now for the HAeBe stars. The polarization is shown in the lower panel while the polarization angle is shown in the upper panel. The black lines denote the best-fitting Serkowski law to the data.

of the dust particles (Whittet et al. 1992). In order to assess whether the observed polarization may have an interstellar dust component, we fit the Serkowski law (equation 3) to our targets and polarized standard stars. λ_{max}, P_{max} and k are taken as a free parameters. The Serkowski law provides – as expected – an excellent fit to the polarized standard stars as shown in Fig. 3. The figure also shows that the polarization angle remains constant over different bands.

The best fit to our targets is provided in Fig. 4. The stars generally follow the Serkowski law but not as well as the standard stars. In some objects, the polarization spectra peak at much longer wavelengths than the V band while, in addition, the polarization angle changes over different bands in all objects. This overall behaviour would suggest that a fraction of the observed polarization is due to interstellar dust, but that an intrinsic contribution is present. This is also consistent with the polarization angle. For all objects, the observed polarization angle changes over different bands, indicating the presence of intrinsic polarization. The deviation of the angle ranges from 1° to 30° (see Fig. 4). The polarized standards did not show a significant deviation in the observed polarization angles.

We note that the continuum polarization and the polarization angle jump from one setting to another for some objects (see Fig. 4). This is particularly striking in PDS 37, R Mon and MWC 275. This might be because the objects are extended, and that a slightly different positioning of the slit could result in slightly different polarization to be measured, which we shall discuss later.

To facilitate comparison with past and future observations, we measured the continuum polarization at the B, V, R and I bands and the results are summarized in Table 2. The linear continuum polarization ranges from ∼0.3 per cent in the very low polarized star HD 85567 to ∼12 per cent in the highly polarized star R Mon. The data of two epochs are provided for three objects, R Mon, V380 Ori and HD 85567. R Mon shows a strong variability of order of ∼4 per cent in the R band between these two epochs. V380 Ori shows similar polarization values and HD 85567 shows a little variation. The literature values for the objects are summarized in Table 3. The polarized standard stars are consistent with the literature values. The HAeBe stars are broadly consistent with the previous measurements, but there is some variation in the polarization data.

Table 3. Previous measured continuum polarization. Column 2 gives the band at which the polarization was measured. Columns 3 and 4 list the measured polarization percentage and polarization angle. The references are presented in the last column.

Object	Band	$P_{cont}(\%)$	θ°_{cont}	Ref.
PDS 37	V	3.253 ± 0.104	120.1 ± 1.0	1
CPD-485215	V	0.348 ± 0.035	20.7 ±3.0	1
R Mon	V	12.0 ± 1.2	91 ± 3	2
	U	11.1 ± 0.7	85.7 ± 1.8	3
	B	11.1 ± 0.4	86.6 ± 1.1	3
	V	12.3 ± 0.5	89.4 ± 1.2	3
	R	12.6 ± 0.3	83.5 ± 0.8	3
	I	12.1 ± 0.4	94.5 ± 0.9	3
V380 Ori	V	0.98 ± 0.10	86 ± 3	2
	R	1.26 ± 0.01	96 ± 1	4
	U	0.08 ± 0.16	151 ± 57	3
	B	0.80 ± 0.06	88.8 ± 2.1	3
	V	0.98 ± 0.06	86.2 ± 1.8	3
	R	1.31 ± 0.14	74.4 ± 3.2	3
	I	1.25 ± 0.18	84.9 ± 4.2	3
BF Ori	R	0.6 ± 0.1	58 ± 1	5
	R	0.886 ± 0.017	52.0 ± 0.6	6
	V	0.46 ± 0.01		7
GU CMa	R	1.15 ± 0.01	19 ± 1	4
	R	0.8 ± 0.1	24 ± 1	5
	R	1.726 ± 0.006	27.0 ± 0.1	6
HD 104237	V	0.032 ± 0.063	167.2 ±56.5	1
HD 85567	V	0.478 ± 0.035	105.7 ± 2.0	1
HD 98922	U	0.515 ± 0.087	152.8 ± 5.0	8
	B	0.201 ± 0.070	168.4 ± 14.1	8
	V	0.235 ± 0.051	160.5 ± 6.0	8
MWC 275	V	0.417 ± 0.035	36.0 ± 2.5	1
	V	0.225 ± 0.012	29.8 ± 1.6	8
	R	0.284 ± 0.014	35.5 ± 1.5	8
	I	0.351 ± 0.018	38.3 ± 1.5	8
	V	0.02 ± 0.01		7

Notes. References. 1: Rodrigues et al. (2009), the errors on the polarization angle for this reference are calculated from 0.5 × arctan ($\sigma p/P$); 2: Hillenbrand et al. (1992); 3: Vrba, Schmidt & Hintzen (1979); 4: Oudmaijer & Drew (1999); 5: Wheelwright et al. (2011); 6: Vink et al. (2005); 7: Oudmaijer et al. (2001); 8: Yudin & Evans (1998), we calculated the average values for MWC 275, taken on the same day.

Table 2. The continuum polarization of the targets measured in the following wavelength regions: B band centred at 4700 Å; V band centred at 5500 Å; R band centred at 7000 Å; I band centred at 9000 Å. The polarization was measured over a wavelength range of 250 Å either side of the central wavelength, except for the B band where it was 125 Å either side. All the errors are differential, where the instrumental error is ∼0.16 per cent in polarization and ∼0.5° in angle (see the text in Section 2.3 for details).

Object	B		V		R		I	
	$P_{cont}(\%)$	θ°_{cont}	$P_{cont}(\%)$	θ°_{cont}	$P_{cont}(\%)$	θ°_{cont}	$P_{cont}(\%)$	θ°_{cont}
PDS 27	8.60 ± 0.03	18.60 ± 0.10	9.00 ± 0.01	18.90 ± 0.01	8.80 ± 0.01	18.40 ± 0.04	7.50 ± 0.01	18.10 ± 0.03
PDS 37	4.70 ± 0.04	130.00 ± 0.30	5.10 ± 0.01	130.80 ± 0.01	5.20 ± 0.01	130.00 ± 0.06	4.40 ± 0.01	133.40 ± 0.05
CPD-485215	1.25 ± 0.01	19.30 ± 0.30	1.30 ± 0.01	15.30 ± 0.06	1.70 ± 0.01	9.50 ± 0.20	1.90 ± 0.01	6.70 ± 0.20
R Mon	11.20 ± 0.04	80.60 ± 0.10	11.20 ± 0.02	80.00 ± 0.05	12.15 ± 0.01	67.70 ± 0.04	12.10 ± 0.01	60.15 ± 0.03
					8.10 ± 0.02	69.40 ± 0.07		
V380 Ori	0.60 ± 0.01	90.80 ± 0.70	0.70 ± 0.01	93.20 ± 0.30	0.70 ± 0.01	98.40 ± 0.06	0.10 ± 0.01	124.00 ± 3.00
V380 Ori	–	–	–	–	0.70 ± 0.02	95.15 ± 1.00	–	–
PDS 133	–	–	–	–	2.30 ± 0.04	37.70 ± 0.50	2.10 ± 0.03	38.30 ± 0.05
BF Ori	–	–	–	–	0.70 ± 0.01	44.00 ± 0.06	–	–
MWC 275	–	–	–	–	0.70 ± 0.01	1.60 ± 0.20	0.67 ± 0.01	14.84 ± 0.28
GU CMa	–	–	–	–	1.60 ± 0.01	14.60 ± 0.01	1.40 ± 0.01	14.45 ± 0.09
HD 104237	–	–	–	–	0.35 ± 0.01	174.60 ± 0.60	0.58 ± 0.01	182.89 ± 0.35
HD 85567	–	–	–	–	0.38 ± 0.01	133.90 ± 0.60	0.23 ± 0.01	154.02 ± 0.61
					0.26 ± 0.02	134.50 ± 2.10		
HD 98922	–	–	–	–	0.40 ± 0.01	174.90 ± 0.30	0.58 ± 0.01	177.90 ± 0.30

The polarization variability in the degree of polarization and/or polarization angle is a common phenomenon among HAeBe objects (Grinin 1994; Jain & Bhatt 1995). Its origin is thought to be caused by the intrinsic polarization over time as the interstellar polarization is unlikely to be variable over a short period of time.

3.2 Line spectropolarimetry

Most of the previous spectropolarimetric studies have been performed on the strong H α emission lines. However, the advantage of this study is that the long spectral coverage allows us to perform linear spectropolarimetry on lines that had never been studied in this manner before. We begin by discussing the results of the strongest hydrogen recombination lines before we discuss other lines.

3.2.1 Hydrogen recombination lines

Spectropolarimetry was performed on all hydrogen lines including H α, H β and the Paschen lines. The spectropolarimetric data around H α are shown in a so-called 'triplot' in the upper half of Fig. 5. In this triplot, the Stokes I (normal intensity) is shown in the lower panel, the polarization percentage in the middle, while the position angle (PA) is shown in the upper panel. The results are also represented in a Stokes (*Q, U)* diagram (bottom) in Fig. 5 using the same wavelength range of the triplot spectra, but sometimes with a different binning. 10 out of the 12 objects display a clear line effect across H α while the remaining two, BF Ori and HD 104237, show a potential line effect. The observed line effects across H α are of order of $\sim$0.2 per cent to $\sim$7 per cent in the case of R Mon. The change in polarization occurs across the emission lines, the absorption components or the entire line profiles.

The spectropolarimetric properties of H α for each target are listed in Table 4. Columns 3–5 list the spectroscopic characterization of Stokes I, the intensity spectrum. Generally, the lines are stronger in HBe objects than in HAe objects. The final three columns represent the line polarimetric properties, i.e. the depolarization, line polarization and McLean effects as introduced in Section 1.

The intrinsic polarization angle is measured from the slope of the loop of the line in the (*Q, U)* diagram following Wheelwright et al. (2011). From the analysis of the (*Q, U)* diagram, we can determine the direction of intrinsic polarization on the sky. We have measured the intrinsic polarization from the slope of the loop across the line in the (*Q, U)* diagram of Fig. 5. This gives two different results depending on the type of the line effect. In the case of line depolarization, the intrinsic angle is measured from the line to continuum while for line polarization it is measured from continuum to the line resulting in a 90° difference from the former. This 90° difference in polarization is equivalent to 180° on the sky, for that reason the direction of the vector in the (*Q, U)* diagram is crucial, and this depends on the type of polarization we observe. For the objects displaying the McLean effect, the angle is measured from the continuum to the line.

The data for the next strongest hydrogen recombination line, H β, is available for five objects. Two of these, R Mon and CPD-485215, show a clear change in polarization across this line and the results are presented in Fig. 6. The Paschen lines are much weaker than the Balmer series and only R Mon shows a line effect across these lines.

3.2.2 Ca II lines

The Ca II triplet at 8498, 8542 and 8662 Å originates at larger distances from the central star than H α because of its lower ionization energy. Only 2 objects out of 12, show a change in polarization across these lines. MWC 275, as shown in Fig. 7, displays a clear change across these lines. The change is as broad as the emission lines and is clear in both polarization and polarization angle. R Mon also shows a change in polarization across these lines (see Fig. A1 in appendix A). PDS 37 shows a possible line effect in only the first two data sets while the second two data sets do not show such a line effect (Ababakr et al. 2015). Therefore, the line effect in PDS 37 is not a conclusive result based on the current data. The Ca II doublet at 8912 and 8927 Å is also seen in the spectra of most objects. R Mon is the only object that shows a line effect across the Ca II doublet.

3.2.3 He I lines

The He I lines trace the very inner hot circumstellar environment as they have a very high excitation energy. Three He I lines at 5876, 6678 and 7065 Å are seen in the spectra of all objects. These lines do not show any signs of a line effect. In most objects the lines are in absorption however, while those in emission are very weak, possibly too weak to show the line effect.

3.2.4 Forbidden lines

Most objects have forbidden emission lines, however line effects across them are limited to a few objects. All the [Fe II] lines show a depolarization in R Mon and CPD-485215. Both [S II] display a clear depolarization in the spectra of R Mon. [O I] lines also display a clear depolarization in R Mon, CPD-485215 and PDS 133. However, the lines are broad and double peaked in PDS 133. The polarization spectra of PDS 133 across [O I] at 6300 Å is presented in Fig. 8 and the remainder of the polarization spectra of all forbidden lines are presented in Fig. A1.

3.2.5 O I and Fe II lines

Two O I lines at 7773 and 8446 Å are observable. R Mon and CPD-485215 show a clear change in polarization across these lines. Several Fe II lines are observable in the spectra of all objects. However, only R Mon shows the line effect across these lines. The polarization spectra can be seen in Fig. A1.

3.2.6 Summary on the occurrence of the line effect

We presented spectropolarimetry from 4560 to 9480 Å of a sample of HAeBe stars that were previously known to have a line effect across the H α line. We find that this phenomenon is very rare across lines other than H α. Strong emission lines such as H β and the Ca II near-infrared triplet are only seen with a line effect in just a few sources. We should perhaps note here that the detection does not necessarily depend on the line strength. For example, lines such as H β and even H γ in the Be star ζ Tau have line effects of order 1 per cent, while the lines themselves hardly reach above the continuum (see the review by Oudmaijer 2007). The fact that strong lines do not exhibit a line effect is thus a very strong observational finding. Finally, R Mon appears to be an exceptional object in the sense that it is the only star in our sample that has a polarization effect in most of its emission lines. We will return to this object later in the following discussion.

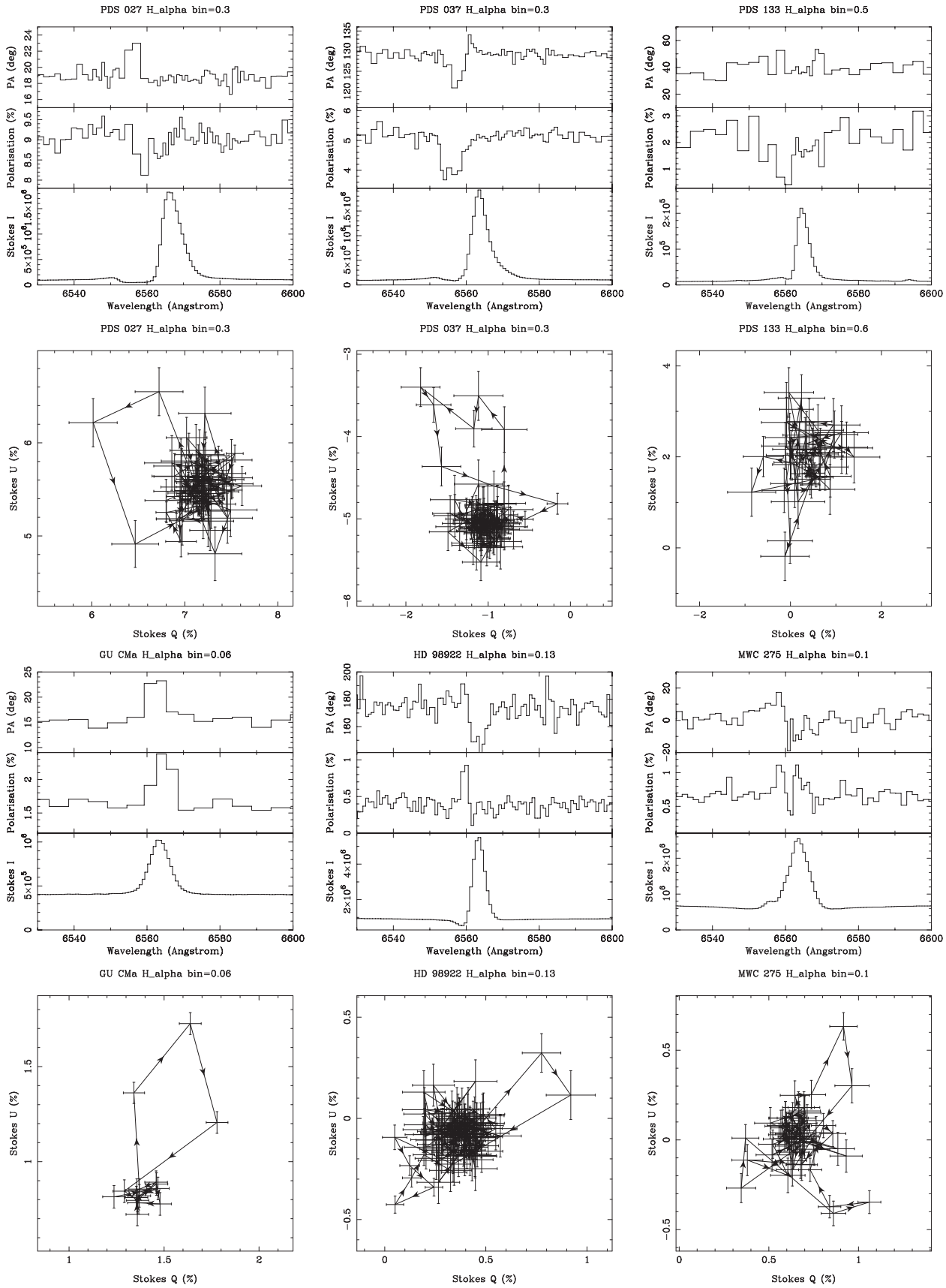

Figure 5. H α spectropolarimetry of the stars. The data are presented as a combination of triplots (top) and (*Q, U)* diagrams (bottom). In the triplot polarization spectra, the Stokes intensity (*I*) is shown in the bottom panel, polarization (per cent) in the centre, while the position angle (PA) is shown in the upper panel. The *Q* and *U* Stokes parameters are plotted against each other below each triplot. The data are rebinned to a constant error in polarization, which is indicated at the top of each plot. The arrows in the (*Q, U)* diagrams indicate the polarization moves in and out of the line effect from blue to red wavelengths.

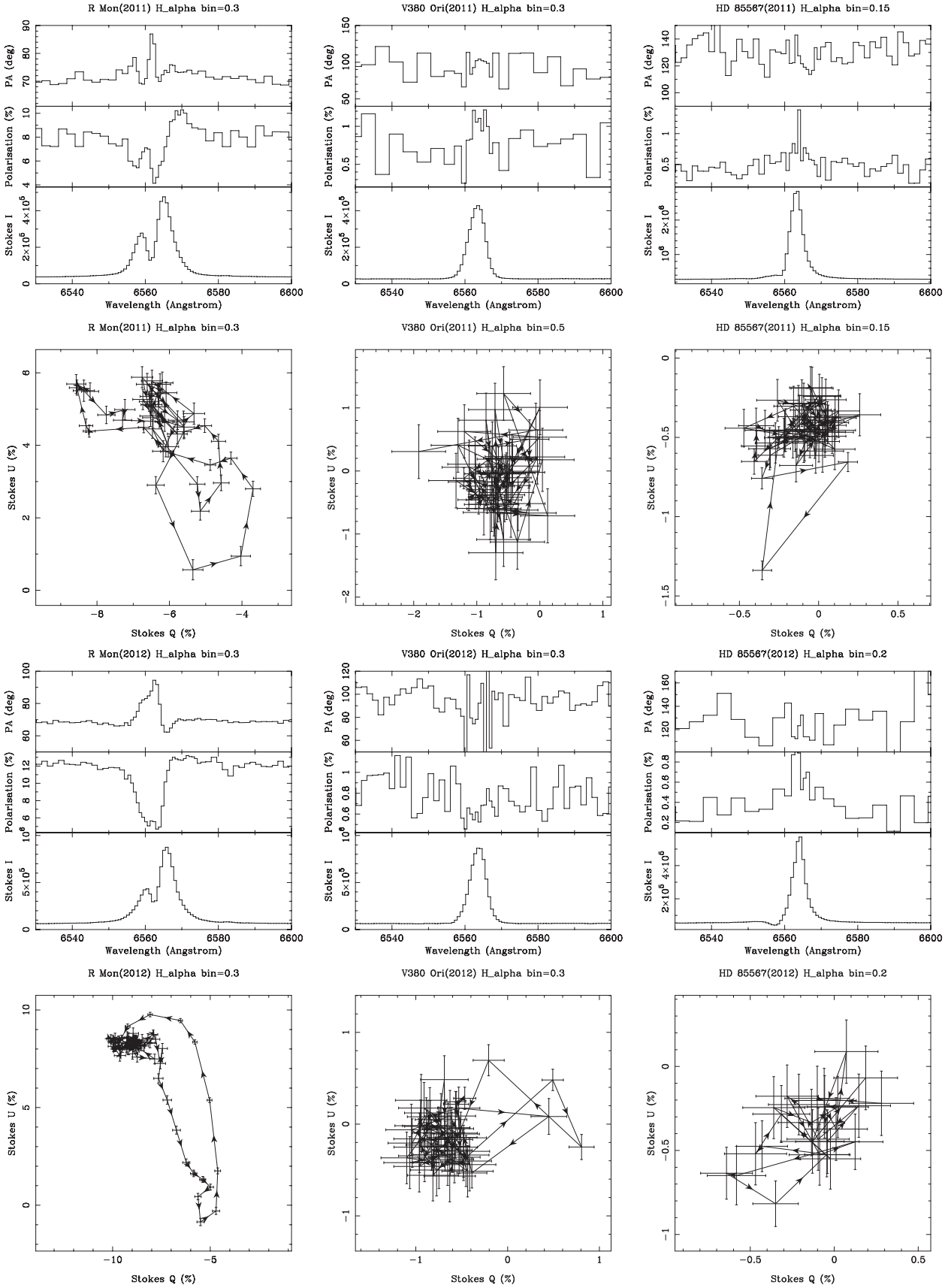

Figure 5 – *continued*

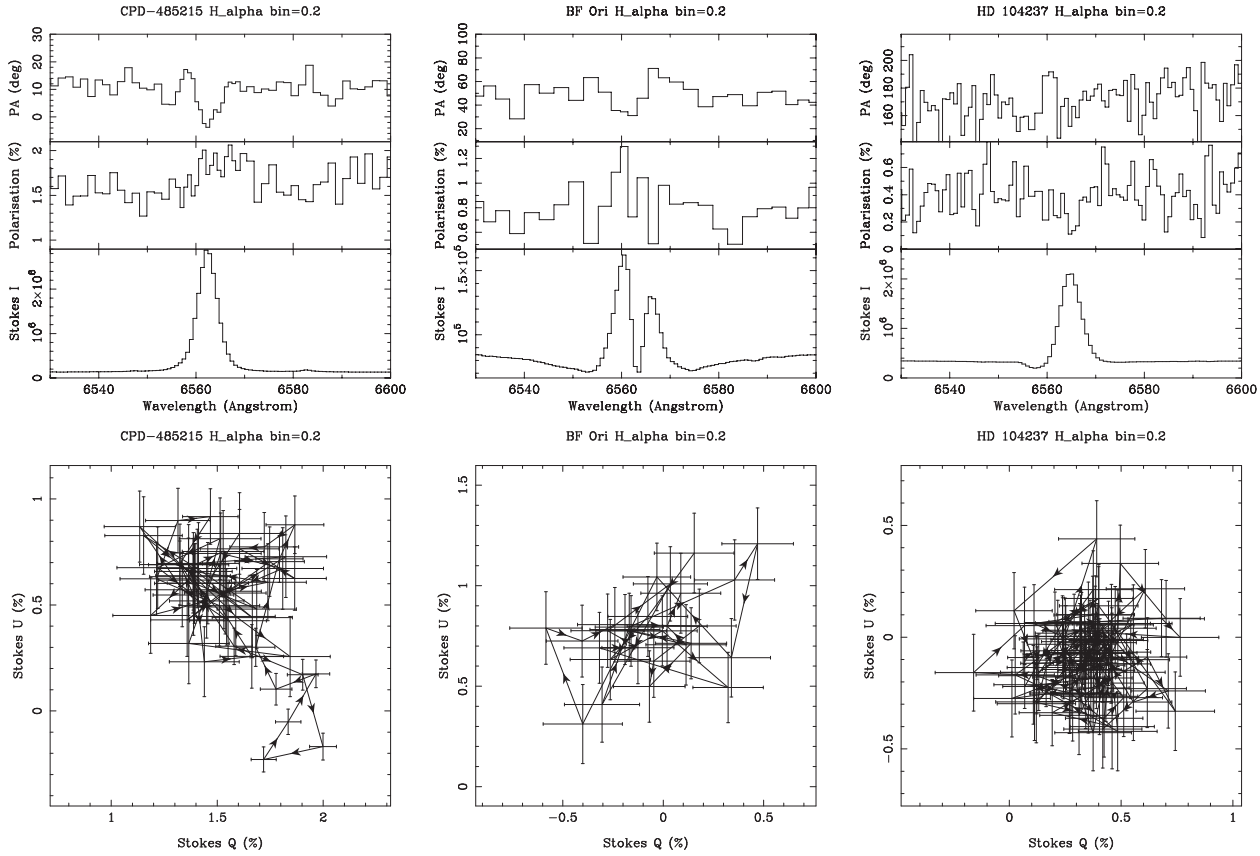

Figure 5 – *continued*

Table 4. The H α line results: columns (3)–(5) list the Stokes (I) characteristics; columns (6)–(8) list line spectropolarimetry characteristics of each target. Column (8) provides an estimation of the intrinsic polarization PA derived from line excursions in the (Q, U) diagram (see the text for details). Errors in the EW measurements are typically 5 per cent, the uncertainty in intrinsic polarization angle is approximately 10°.

Object	Spec. type	Line profile	EW (Å)	Line/cont.	Line effect	Classification	$\theta^{\circ}_{\rm intr}$
PDS 27	B3	P Cygni	−120.8	18.0	Yes	McLean	77
PDS 37	B3	P Cygni	−122.6	19.4	Yes	McLean	56
PDS 133	B6	P Cygni	−94.5	20.7	Yes	McLean	126
HD 98922	A0	P Cygni	−17.9	6.0	Yes	McLean\Depol.	22
R Mon(2011)	B8	Double-peaked	−98.6	12.6	Yes	Depol.	63
R Mon(2012)	–	Double-peaked	−105.5	12.9	Yes	Depol.	57
GU CMa	B1	Pure emission	−11.1	2.6	Yes	Depol.	127
CPD-485215	B6	Pure emission	−100.8	19.6	Yes	Depol.	62
MWC 275	A1	P Cygni	−14.9	3.8	Yes	∼ Pol.	112
HD 85567(2011)	B7	P Cygni	−43.5	9.9	Yes	∼ Depol.	31
HD 85567(2012)	–	P Cygni	−42.1	10.2	Yes	∼ Depol.	22
V380 Ori(2011)	A0	Pure emission	−82.7	15.5	Possible	–	–
V380 Ori(2012)	–	Pure emission	−71.1	13.6	Yes	∼ pol.	10
HD 104237	A7	P Cygni	−27.2	6.5	Possible	–	–
BF Ori	A2	Double-peaked	1.0	1.9	Possible	–	–

4 ANALYSIS

The spectropolarimetric results of the sample show a continuum polarization at the level between ∼0.3 per cent to ∼12 per cent. Unlike the polarized standard stars, the majority of objects do not follow the empirical curve of the Serkowski law. A line effect is present across the H α line in all objects.

We observe three different line effects across the H α line in the sample (see Table 4): depolarization, intrinsic polarization; and a polarization change across the absorption, which is commonly

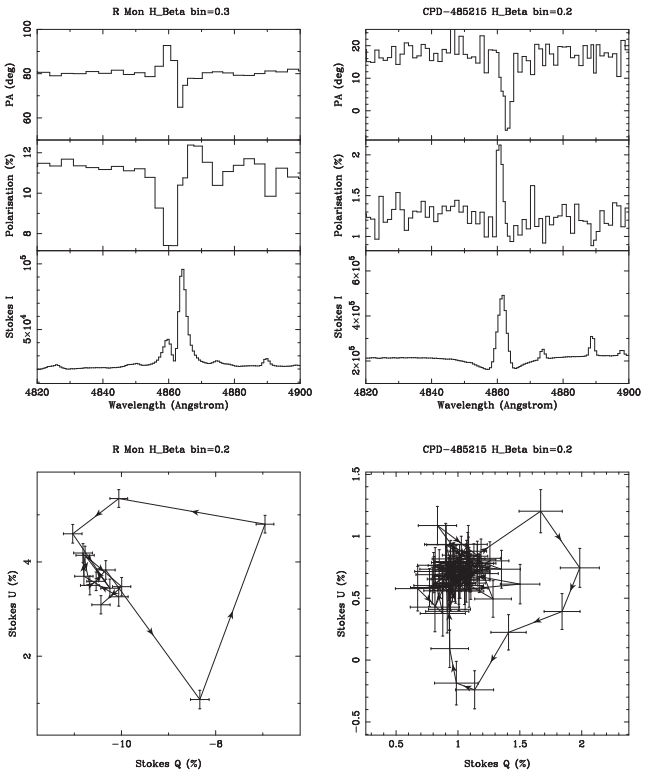

Figure 6. H β spectropolarimetry of R Mon and CPD-485215. See the caption of Fig. 5 for more details.

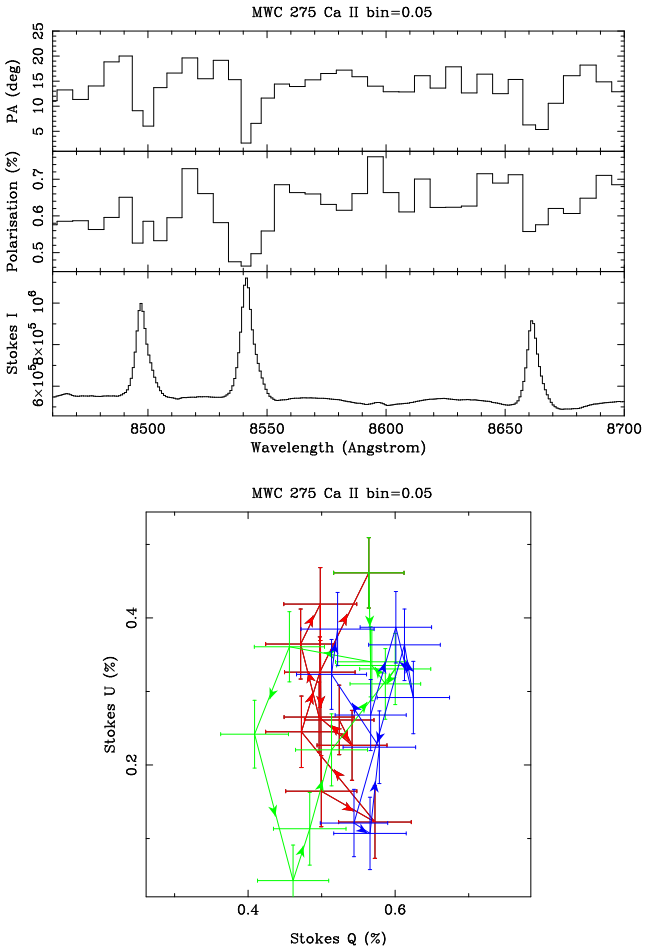

Figure 7. Ca II triplet polarization data of MWC 275. In the (*Q, U*) diagram, the lines at 8498, 8542 and 8662 Å are plotted in red, green and blue solid lines. See the caption of Fig. 5 for more details.

referred to as the McLean effect. In depolarization, the polarization across the emission line decreases compared to the continuum, and it is more common in high mass stars (Clarke & McLean 1974; Poeckert & Marlborough 1976). Intrinsic line polarization can be due to an anisotropic line emitting region scattering off circumstellar material, and it was found in T Tauri and HAe stars (Vink et al. 2002, 2003, 2005). The McLean effect is where the absorption component of the emission line often has a different polarization than the continuum, but the emission has not (McLean 1979). There is a distinct difference in polarimetric properties between the HBe stars, showing depolarization and the HAe stars showing enhanced polarization across the line.

The intrinsic line polarization is thought to be caused by the effects of magnetospheric accretion. In this case, disc material is funnelled through accretion columns on to the stars. The material shocks the photosphere where it crashes into at high speeds. The line emission coming from these hotspots will be polarized as they scatter off the disc material, which becomes detectable as a line effect (Vink, Harries & Drew 2005).

4.1 McLean effect

A number of objects display a polarization change across the P Cygni absorption of the hydrogen lines and do not necessarily fit into the categories above.

The concept of the McLean effect is based on the fact that the wind material in our line of sight blocks the unscattered light and removes it from the beam. This leads to observation of a strong emission line with a blueshifted absorption component. However, the flux in the absorption does not reach zero because the re-emission process is isotropic; some of the photons will be scattered into our line of sight. If the distribution of the scattering material is aspherical, the observed light across the absorption will be more polarized than the continuum light. PDS 27, PDS 37 and PDS 133 show a clear McLean effect across the absorptive component of H α. The line effect is of order 1–2 per cent in these objects. Naively, we might expect the same line effect across the H β but this is not observed. Fig. 9 shows the H α and H β P Cygni profile of PDS 27, PDS 37 and PDS 133. The P Cygni absorption seems to be saturated with broad and flat core features for PDS 27 and the absorption is around 0.4 and 0.15 of the continuum level for H α and H β, respectively. In PDS 37, the P Cygni absorption is at 0.75 and 0.3 of the continuum level for H α and H β, respectively. The absorption in H β is thus deeper than that of H α in both objects. This is not expected as typically the higher lines display weaker absorption. This unusual behaviour is also seen for the Paschen lines as presented in Fig. 10. The figure shows that the absorption component of Pa β is weaker than Pa γ and Pa δ. Unlike PDS 27 and PDS 37 the absorption part of the line of PDS 133 is above the continuum.

By analysing the observed P Cygni spectral lines and the observed polarization line effects, we can understand the McLean effect in H α and its absence in H β relatively straightforwardly. The strong H α line photons are scattered into the line of sight filling in the absorption component. If the scattering region is a-symmetric, net polarization across the absorption part of the line will be observable.

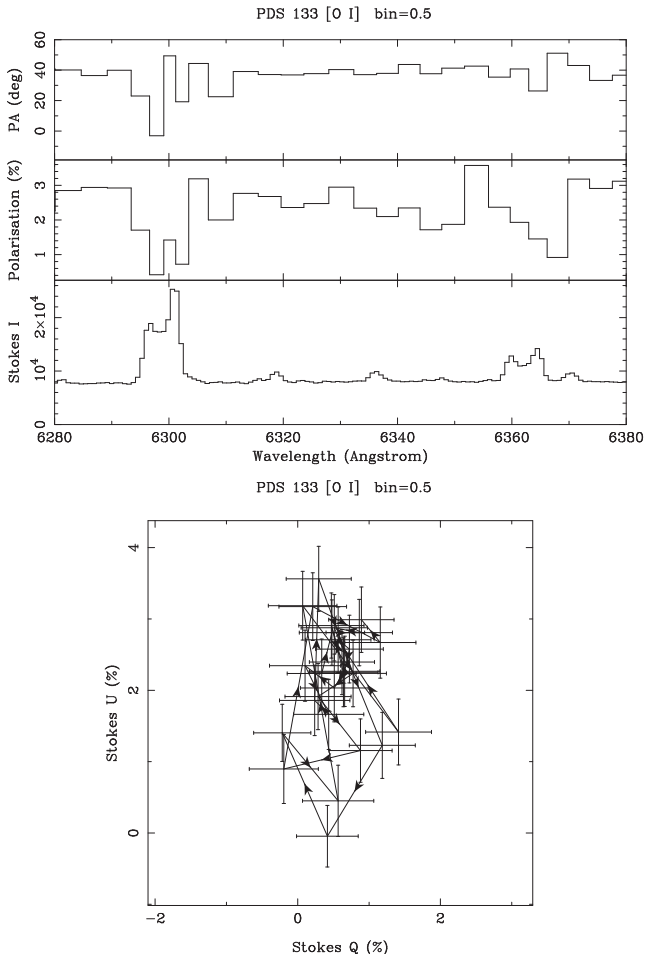

Figure 8. [O I] at 6300 and 6364 Å polarization data of PDS 133. See the caption of Fig. 5 for more details.

The H β line, which is weaker than H α has fewer photons, and will therefore also have fewer scattered photons filling the absorption component (see Fig. 9). The net effect is that both the H β absorption remains deeper than for H α, while the scattered, polarized component is less obvious. Therefore, the lack of the scattered photons in H β could explain the absence of the line effect across this line. This argument is supported by the observed line effects across the absorptive component of H α in PDS 27, PDS 37 and PDS 133, as the line effect is stronger for a weaker absorption component. Ababakr et al. (2015) suggested a similar scenario in an in-depth study of PDS 27 and PDS 37, but here we have an extra object that follows the same pattern.

For illustration, we sketch the situation in Fig. 11. In the schematic we can see that different levels of polarization in the line of sight result in different absorption line profiles. In the case of large polarization, we do not see any absorption in the observed line profile as the polarized light fills in the absorption. Interestingly, the McLean effect can thus also be observed in the absence of absorption. In contrast, very deep absorption would be observed when there is little or no polarization.

4.2 The case of R Mon

A small number of objects display line effects across more lines than H α alone. We discuss these here, focusing on the most extreme object, R Mon. Its continuum polarization is large, with values of order 12 per cent and 8 per cent, in the *R* band in 2012 and 2011, respectively. Unlike the other stars, R Mon displays a line effect across virtually all observed emission lines. The difference between line and continuum polarization is 7 per cent across the H α and H β lines (see Figs 5 and 6), which is large and rare. Typically, the strongest line effect due to electron scattering is of order 2 per cent (Oudmaijer 2007). In addition, the direction of the intrinsic polarization angle from the line effects in the *(Q, U)* diagram is not constant over different bands. Therefore, it would appear that R Mon is atypical as it differs on many counts from most objects that have been studied spectropolarimetrically.

Relevant to this discussion is that R Mon is an extended object. Its reflection nebula is due to radiation from the inner parts, such as the star and wind, being scattered off circumstellar dust particles, resulting in strong polarization. Spatially resolved polarization images reveal polarization in excess of 50 per cent (Jolin et al. 2010). The polarized flux is largest closest to the star and decreases with distance, while the polarization angles follow a centro-symmetric pattern. For a circularly symmetric, highly polarized object on the sky, the same would apply, but if it were unresolved, the net observed polarization would be zero. However, because R Mon is asymmetric, a net polarization will be observed, and this is even stronger in our data as the scattering circumstellar material is resolved and larger than the slit.

These features have important consequences for the observed polarimetry. Below we will argue that this is the main reason that the (spectro-)polarimetric properties of R Mon are different from the other stars, and that the various emission lines originate from different line forming regions. For example, given that the polarization drops off rapidly with distance from the star, a slight change in seeing or slight change in the positioning of the slit can result in largely different polarized light entering the slit. In addition, larger positioning errors can result in differently observed position angles, as the PA depends on position.

Inspection of the raw spectropolarimetric data shows that the width of the ordinary (O) and extraordinary (E) beam in the spatial direction in the 2011 data is about twice that of the 2012 data (and wider than the data for the other stars). In addition, the individual beams do not follow the typical Gaussian shape of the seeing profile, but appear asymmetric. This confirms that R Mon is not a point source but an irregular, extended object.

Let us discuss the polarization properties of R Mon in this context, starting with its observed broad-band peculiarities. The polarization seemingly increased by 4 per cent over a timespan of 4 months, while the polarization angle stayed the same. The slit direction and position were the same for both observations but as mentioned above, the spatial profile of the 2011 data, which has a smaller level of polarization, is much wider than that in 2012. As the polarization closest to the object is highest, it follows that the net polarization in 2012 is higher. A similar argument can be put forward to explain the discrepant position angles for each of the wavebands the object was observed. In Fig. 4, the slope of the PA is the same for the *V*, *R* and *I* bands, but they are offset by 10° (see also Table 2). According to the data in Jolin et al. (2010), the polarization is centro-symmetric, and the polarization angle changes with at least 20° every 1 arcsec. Hence, a slight displacement can result in a noticeable change in PA. We argue, therefore, that the fact that R Mon is extended and asymmetric explains the high polarization, large continuum variability, and offset in PA for the various wavelength settings.

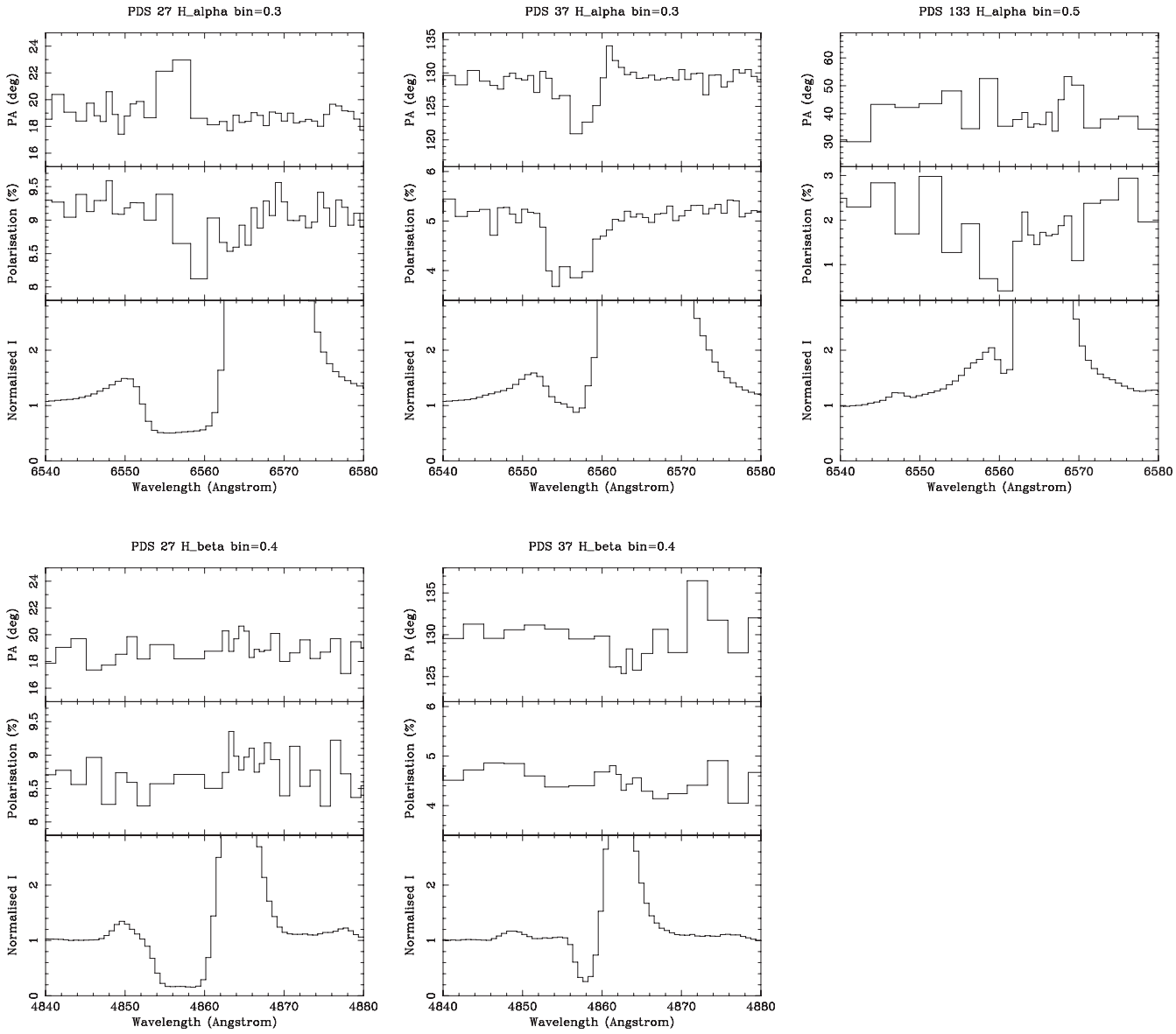

Figure 9. H α and H β spectropolarimetry of PDS 27, PDS 37 and PDS 133. For PDS 133 only H α data is available. See the caption of Fig. 5 for more details.

Let us now turn to the spectropolarimetric properties, of which the fact that most lines seem to exhibit a line effect, and that the line effect is large, makes R Mon stand out.

The left-hand panel of Fig. 12 shows the (*Q, U*) diagram of three forbidden lines of R Mon, with each line taken from a different wavelength setting. The right hand panel shows lines from different wavelength settings as well; H β, H α and a Ca II triplet line, at 8662 Å. The line excursions are large, ranging from ∼5 per cent to ∼10 per cent in H α. The direction of the intrinsic polarization angle is roughly the same for all forbidden lines, with an average value of 64 ± 5°. However, very different intrinsic angles of 90 ± 15°, 57 ± 10° and 128 ± 10° are found for H β, H α and the Ca II triplet line, respectively. The H α and Ca II triplet data were taken at the same date while H β was taken a few days later. The polarization angle in H α is the only one consistent with the forbidden lines.

The question that now arises is how can the line effects be strong, and why would the intrinsic angles be different for the various lines? By simply stating that the lines are formed in a larger region than the star and would be less prone to scattering, such as the polarization dilution discussed in Trammell, Dinerstein & Goodrich (1994), does not hold in the current situation. The reflecting dust is located far away from the star and is in all likelihood much more extended than the ionized wind. In this case, the emission lines will be equally likely to be scattered and thus as polarized as the continuum. The remaining possibility is that the line emitting regions themselves are not isotropic – either asymmetric or clumpy, leading to a polarization line emission different from the continuum. The different polarization angles for the various lines may be the result of different geometries and volumes of the line forming regions. The optically thick H α emission and the forbidden lines originate from large, possibly similar volumes, which could follow similar

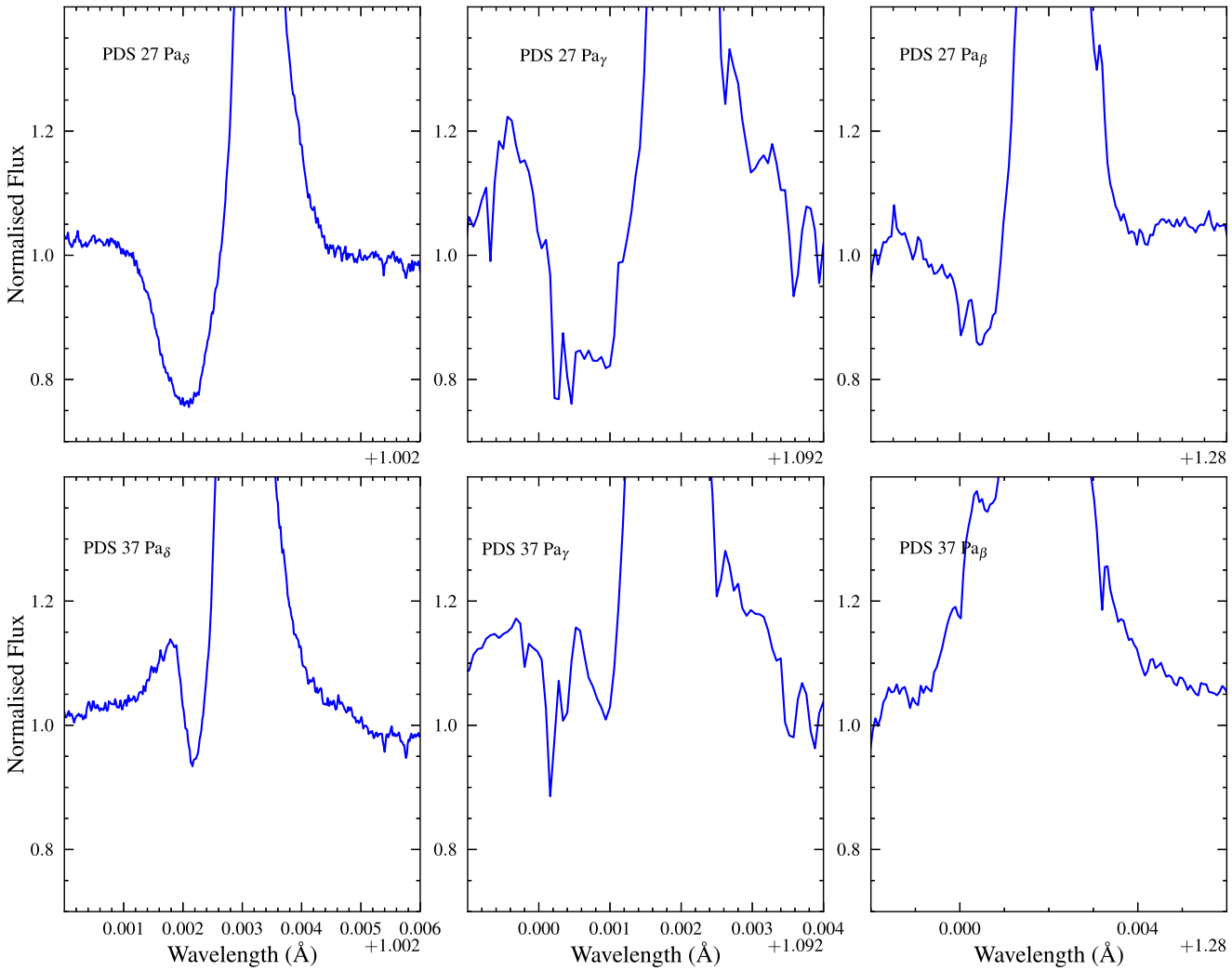

Figure 10. The comparison of P Cygni profile, Pa δ, Pa γ and Pa β of PDS 27 and PDS 37. The spectroscopic data are taken from the HAeBe X-shooter project (Oudmaijer et al. 2011; Fairlamb et al. 2015).

scattering paths, whereas other lines arise in regions closer to the star and have potentially different geometries, leading to different polarization angles.

To our knowledge this is the first time an object has been reported to have so many lines with a polarization effect across them. It will not be trivial to disentangle the various contributions and multi-parameter modelling is needed to retrieve the geometry of the system. This is beyond the scope of the current paper.

5 FINAL REMARKS AND CONCLUSIONS

We have performed the first linear spectropolarimetry over a large wavelength range of a sample of HAeBe stars. The spectra cover the range from 4560 to 9480 Å, including many emission lines such as: hydrogen recombination lines, Ca II, Fe II, O I and He I and several forbidden lines including [O I], [Fe II] and [S II]. All the objects have a measurable continuum polarization, ranging from ∼0.3 per cent in the very low polarized star HD 85567 to ∼12 per cent in the highly polarized star R Mon. Our values are broadly consistent with these values but there are some variations from the literature values. The continuum polarization of some of our objects do not follow the general trend of the Serkowski law. This is evidence of the presence of intrinsic polarization in the observed continuum polarization as the interstellar polarization does not vary significantly over time.

All the objects show a sign of line effect across H α. All HBe objects display either a classical depolarization or a McLean effect signature. The HAe objects show a mixture of McLean, depolarization, intrinsic line polarization and complex line effect. This suggests that the circumstellar environments around HAeBe stars have a flattened structure. Four objects in our sample show a McLean effect, where the change in polarization occurs across the absorptive component of the emission line of H α. This suggests that the distribution of the ionized material is not circular on the sky. From these four objects we only have Hβ data for PDS 27 and PDS 37. We would expect the same line effect across the absorption component of H β. However, the absorption in H β is approximately three times stronger than that of H α. We can explain this apparent inconsistency by the fact that strong H α line emission scatters into our line of sight filling in the absorption component. The H β

line is weaker than H α and thus fewer scattered photons fill in the absorption component, yielding a much lower polarization effect, consistent with the observed non-detection.

It would appear, therefore, that we can explain the differing polarization behaviour across the absorption parts of the H α and H β lines very well in the context of the McLean effect. An alternative scenario to explain polarization across the absorption parts of hydrogen lines was put forward by Kuhn et al. (2007). Essentially this invokes selective optical pumping of the lines, predicting that both H β and H α will have polarization effects of roughly similar magnitude (Kuhn et al. 2011, their figs 4 and 5). This is not what we observe in our data. What is more, this scenario will also struggle to explain why the H β absorption is so much stronger than that of H α. Within the current set of observations, the McLean effect seems to be a more viable explanation.

Four HBe objects show a depolarization line effect, where the change in polarization is as broad as the emission line. This suggests that H α emerge in an extended circumstellar disc. Two HAe objects show an intrinsic line polarization, where a significant portion of the photons emerge from accretion hotspots. BF Ori and HD 104237 show a possible line effect across Hα.

We have observed depolarization line effects across [O I] lines at 6300 and 6364 Å in PDS 133, R Mon and CPD-485215. The line profile in PDS 133 is broad and double peaked unlike the other two, which are narrow and single peaked. The line profiles may suggest that the lines originate from a rotating disc in PDS 133 while in R Mon and CPD-485215 many forbidden lines display a depolarization line effect. It is to be expected to see a depolarization line effect across [O I] in PDS 133 as they originate in the disc further out from the inner ionized disc. The Ca II triplet also shows a depolarization in MWC 275. These lines have low ionization potential energy as they are formed in a predominately neutral zone. In general they originate in the circumstellar environment but outside the hydrogen ionization boundary. Therefore, we might expect a depolarization line effect across these lines. However, for the objects that display a depolarization line effect, the Ca II triplet line effects are either absent or very weak.

Finally, we have presented the medium resolution spectropolarimetry on the entire optical range from 4560 to 9480 Å of a sample of 12 HAeBe stars. The data allow us to draw the following conclusions:

(i) We sample linear line spectropolarimetry in the optical wavelength range, which is much larger than any previous work at similar spectral resolution.

(ii) Changes in the polarization across the H α emission line are detected in all objects, as an indication of a flattened structure of the circumstellar environment. The line effects vary from depolarization, line polarization to the McLean effect.

(iii) Depolarization and the McLean effect are observed in Be type stars predominantly in early B type stars while line polarization is observed in Ae type objects.

(iv) The McLean effect is observed only across the absorptive component of H α and the line effect is stronger for a weaker absorption component, while H β does not display the effect. We propose a scenario to explain this property. It is based on the fact that the photons from the strong H α line are scattered into the line of sight. As a consequence, the photons in the absorption are more polarized than the emission. A side result is that the selective absorption due to optical pumping as proposed by Kuhn et al. (2007) is unlikely to be responsible for the polarization behaviour in these objects.

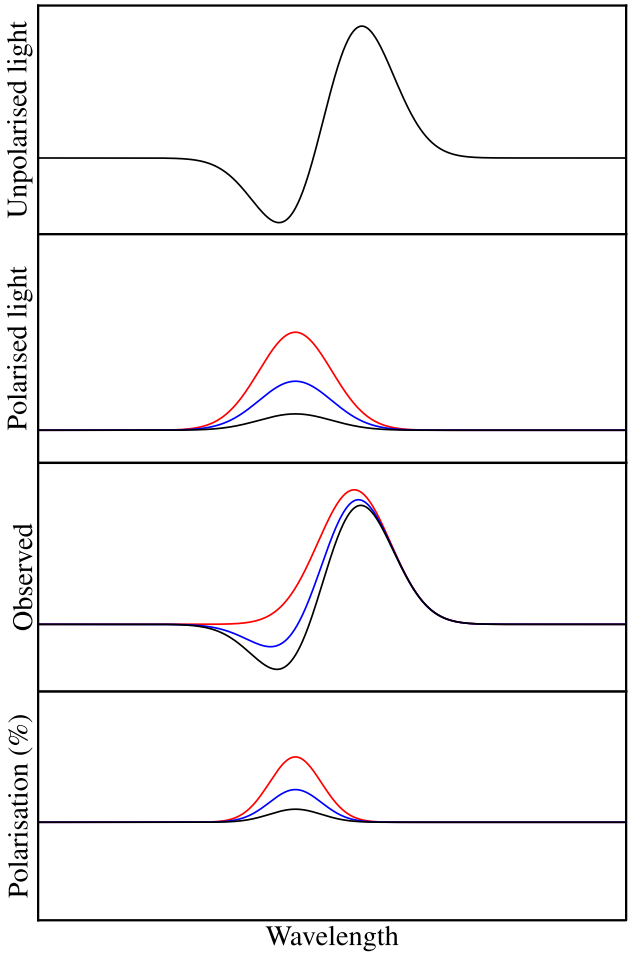

Figure 11. Schematic explaining the McLean effect with the data present in three sets: the unpolarized light is shown in the upper panel, polarized light into the line of sight in the upper middle, the observed H α line profile in the lower middle and the observed polarization (per cent) is shown in the lower panel. The absorption is completely filled when there is a significant amount of polarization in our line of sight, this results in a detection of a notable line effect (red solid line). In contrast, when the polarized light into our line of sight is not sufficient to fill in the absorption component significantly, this results in a weak line effect which is challenging to observe (black solid line). The solid blue line represents an average between the two extreme cases.

(v) We detect a broad depolarization line effect across Ca II triplet and [O I] in two objects. These lines are emerging further away from the star and H α region in the circumstellar environment. The depolarization simply implies that the circumstellar environment has an asymmetrical structure in this region.

(vi) The few spectra with calcium triplet lines that show an effect show a similar polarization profile for all members of the triplet. We confirm a similar observation by Kuhn et al. (2011) for an evolved, RV Tau star. As these authors explained, resonant line scattering can then not be the cause for the observed line polarization, as the Ca II 8662 Å comes from a different upper level than the other members of the triplet. Similar polarization due to line scattering would then not be expected.

(vii) Finally, apart from H α, few lines in few objects show a line effect in the polarization. We present the case of R Mon, which

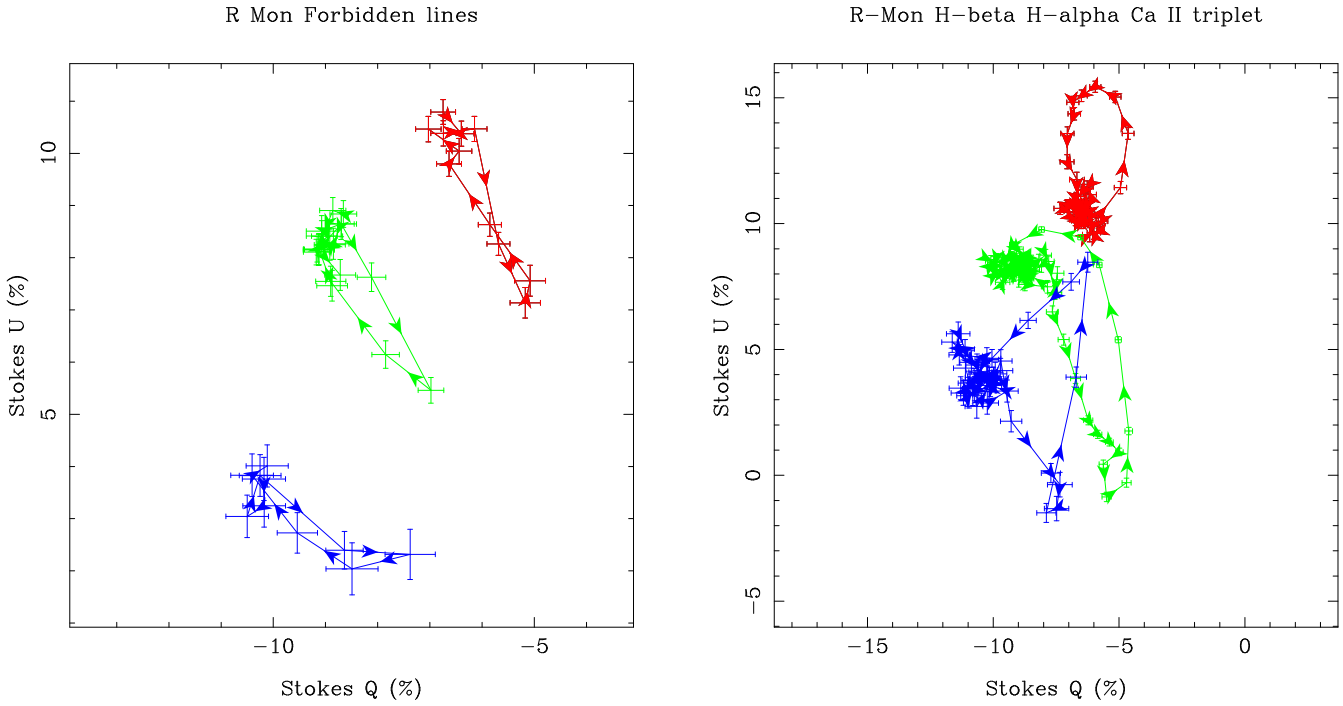

Figure 12. (*Q, U*) diagram of several spectral lines and forbidden lines of R Mon. The lines are taken from *B* band (blue solid line), *R* band (green solid line) and *I* band (red solid line). H β, H α and Ca II triplet at 8662 Å are presented in blue, green and red lines respectively (right); three forbidden lines: [Fe II] at 5158 Å, [O I] at 6364 Å and [Fe II] at 8616 Å are shown in blue, green and red lines, respectively (left).

displays exceptionally strong line effects in most of its emission lines. In addition, not all lines show the same type of line effect. We explain this by the fact that the object itself is resolved and propose that different line forming regions and geometries are responsible for polarization properties of the higher hydrogen recombination lines and forbidden lines and H α on the other hand.

ACKNOWLEDGEMENTS

We are very grateful to the referee, Richard Ignace, for his constructive and very insightful remarks that helped us improve the paper. This research has made use of the SIMBAD data base, operated at CDS, Strasbourg, France.

REFERENCES

Ababakr K. M., Fairlamb J. R., Oudmaijer R. D., van den Ancker M. E., 2015, MNRAS, 452, 2566
Acke B., van den Ancker M. E., Dullemond C. P., 2005, A&A, 436, 209
Beltrán M. T., de Wit W. J., 2016, A&AR, 24, 6
Clarke D., McLean I. S., 1974, MNRAS, 167, 27
Fairlamb J. R., Oudmaijer R. D., Mendigutía I., Ilee J. D., van den Ancker M. E., 2015, MNRAS, 453, 976
Fossati L., Bagnulo S., Mason E., Landi Degl'Innocenti E., 2007, in Sterken C., ed., The Future of Photometric, Spectrophotometric and Polarimetric Standardization, ASP Conf. Ser. Vol 364, Standard Stars for Linear Polarization Observed with FORS1. Astron. Soc. Pac., San Francisco, p. 503
Grady C. et al., 2015, Ap&SS, 355, 253
Grinin V. P., 1994, in The P. S., Perez M. R., van den Heuvel E. P. J., eds, The Nature and Evolutionary Status of Herbig Ae/Be Stars, ASP Conf. Ser. Vol. 62, Polarimetric activity of Herbig Ae/Be stars. Astron. Soc. Pac., San Francisco, p. 63
Harries T. J., 1996, Starlink User Note, 204
Herbig G. H., 1960, ApJS, 4, 337
Hillenbrand L. A., Strom S. E., Vrba F. J., Keene J., 1992, ApJ, 397, 613
Ignace R., Brimeyer A., 2006, MNRAS, 371, 343
Ilee J. D., Fairlamb J., Oudmaijer R. D., Mendigutía I., van den Ancker M. E., Kraus S., Wheelwright H. E., 2014, MNRAS, 445, 3723
Jain S. K., Bhatt H. C., 1995, A&AS, 111, 399
Jolin M.-A., Bastien P., Denni F., Lafrenière D., Doyon R., Voyer P., 2010, ApJ, 721, 1748
Kraus S., 2015, Ap&SS, 357, 97
Kuhn J. R., Berdyugina S. V., Fluri D. M., Harrington D. M., Stenflo J. O., 2007, ApJ, 668, L63
Kuhn J. R., Geiss B., Harrington D. M., 2011, in Kuhn J. R., Harrington D. M., Lin H., Berdyugina S. V., Trujillo-Bueno J., Keil S. L., Rimmele T., eds, Solar Polarization 6, ASP Conf. Ser. Vol. 437, Using Absorptive Linear Polarization Spectroscopy to Understand Imbedded Stars. Astron. Soc. Pac., San Francisco, p. 245
McLean I. S., 1979, MNRAS, 186, 265
Mottram J. C., Vink J. S., Oudmaijer R. D., Patel M., 2007, MNRAS, 377, 1363
Muzerolle J., Calvet N., Hartmann L., 1998, ApJ, 492, 743
Oudmaijer R. D., 2007, in Hartquist T. W., Falle S. A. E. G., Pittard J. M., eds, Diffuse Matter from Star Forming Regions to Active Galaxies. Springer-Verlag, Berlin, p. 83
Oudmaijer R. D., Drew J. E., 1999, MNRAS, 305, 166
Oudmaijer R. D., Proga D., Drew J. E., de Winter D., 1998, MNRAS, 300, 170
Oudmaijer R. D. et al., 2001, A&A, 379, 564
Oudmaijer R. D. et al., 2011, Astron. Nachr., 332, 238
Poeckert R., Marlborough J. M., 1976, ApJ, 206, 182
Quirrenbach A., Buscher D. F., Mozurkewich D., Hummel C. A., Armstrong J. T., 1994, A&A, 283, L13
Rodrigues C. V., Sartori M. J., Gregorio-Hetem J., Magalhães A. M., 2009, ApJ, 698, 2031
Serkowski K., Mathewson D. S., Ford V. L., 1975, ApJ, 196, 261

The P. S., de Winter D., Perez M. R., 1994, A&AS, 104, 315
Tody D., 1993, in Hanisch R. J., Brissenden R. J. V., Barnes J., eds, Astronomical Data Analysis Software and Systems II, ASP Conf. Ser. Vol. 52, IRAF in the Nineties. Astron. Soc. Pac., San Francisco, p. 173
Trammell S. R., Dinerstein H. L., Goodrich R. W., 1994, AJ, 108, 984
Vieira S. L. A., Corradi W. J. B., Alencar S. H. P., Mendes L. T. S., Torres C. A. O., Quast G. R., Guimarães M. M., da Silva L., 2003, AJ, 126, 2971
Vink J. S., 2015, Ap&SS, 357, 98
Vink J. S., Drew J. E., Harries T. J., Oudmaijer R. D., 2002, MNRAS, 337, 356
Vink J. S., Drew J. E., Harries T. J., Oudmaijer R. D., Unruh Y. C., 2003, A&A, 406, 703
Vink J. S., Drew J. E., Harries T. J., Oudmaijer R. D., Unruh Y., 2005, MNRAS, 359, 1049
Vink J. S., Harries T. J., Drew J. E., 2005, A&A, 430, 213
Vrba F. J., Schmidt G. D., Hintzen P. M., 1979, ApJ, 227, 185
Wheelwright H. E., Vink J. S., Oudmaijer R. D., Drew J. E., 2011, A&A, 532, A28
Wheelwright H. E., Bjorkman J. E., Oudmaijer R. D., Carciofi A. C., Bjorkman K. S., Porter J. M., 2012, MNRAS, 423, L11
Whittet D. C. B., Martin P. G., Hough J. H., Rouse M. F., Bailey J. A., Axon D. J., 1992, ApJ, 386, 562
Yudin R. V., Evans A., 1998, A&AS, 131, 401

APPENDIX A: OBSERVED POLARIZATION IN THE OPTICAL RANGE FROM ∼4600 Å TO ∼9400 Å FOR ALL OBJECTS

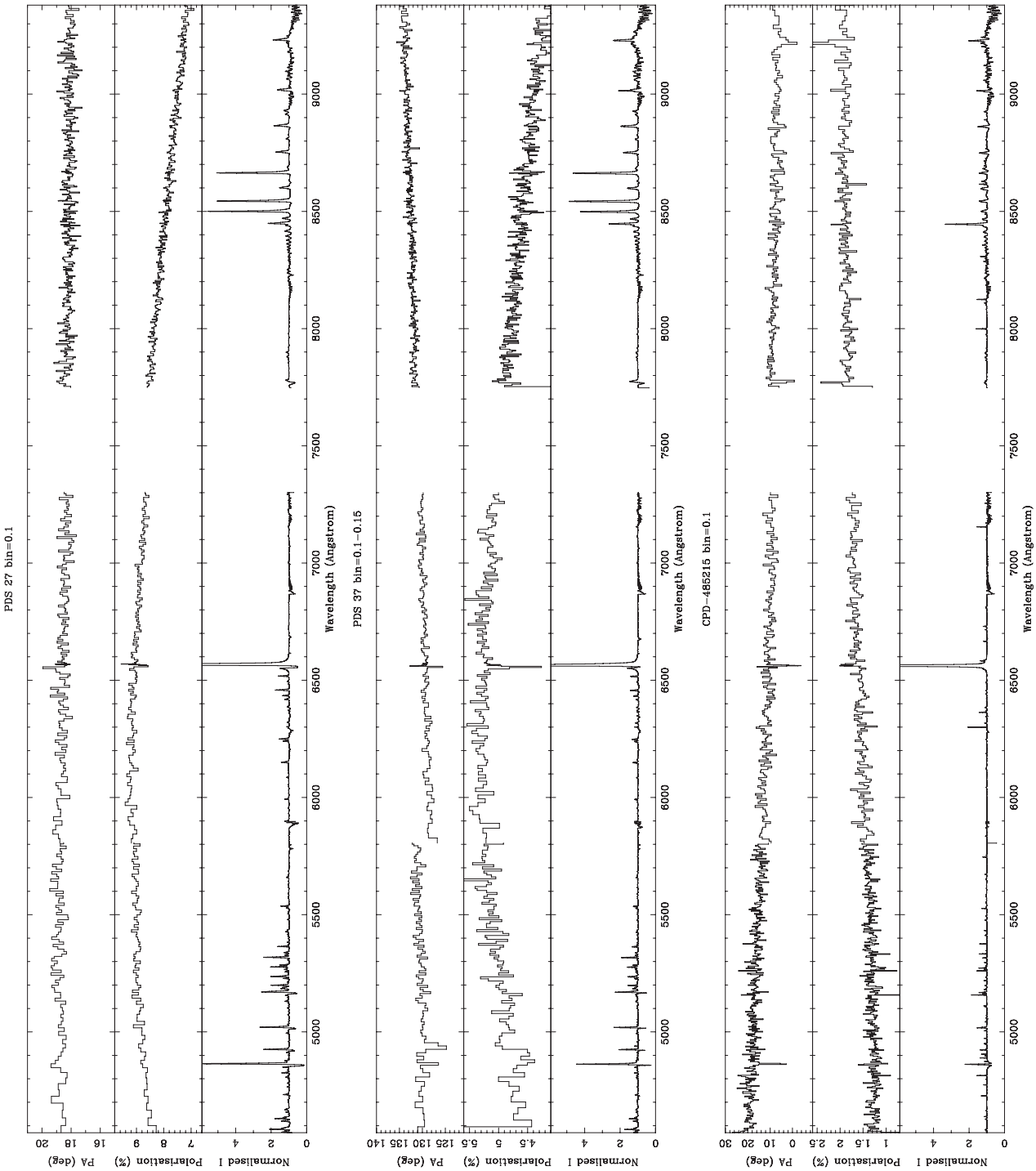

Figure A1. The polarization data in *V*, *R* and *Z* bands for PDS 27, PDS 37,CPD-485215, R Mon and V380 Ori; and in *R* and *Z* bands for GU CMa, HD 98922, PDS 133, HD 104237, MWC 275, BF Ori and HD 85567. R Mon, V380 Ori and HD 85567 are presented in two epochs in *R*. The data are presented as a triplots. In the triplot polarization spectra the Stokes intensity (*I*) is shown in the lower panel, polarization (per cent) in the centre, while the position angle (PA) is shown in the upper panel. The data are rebinned to a constant value, as indicated at the top of each plot.

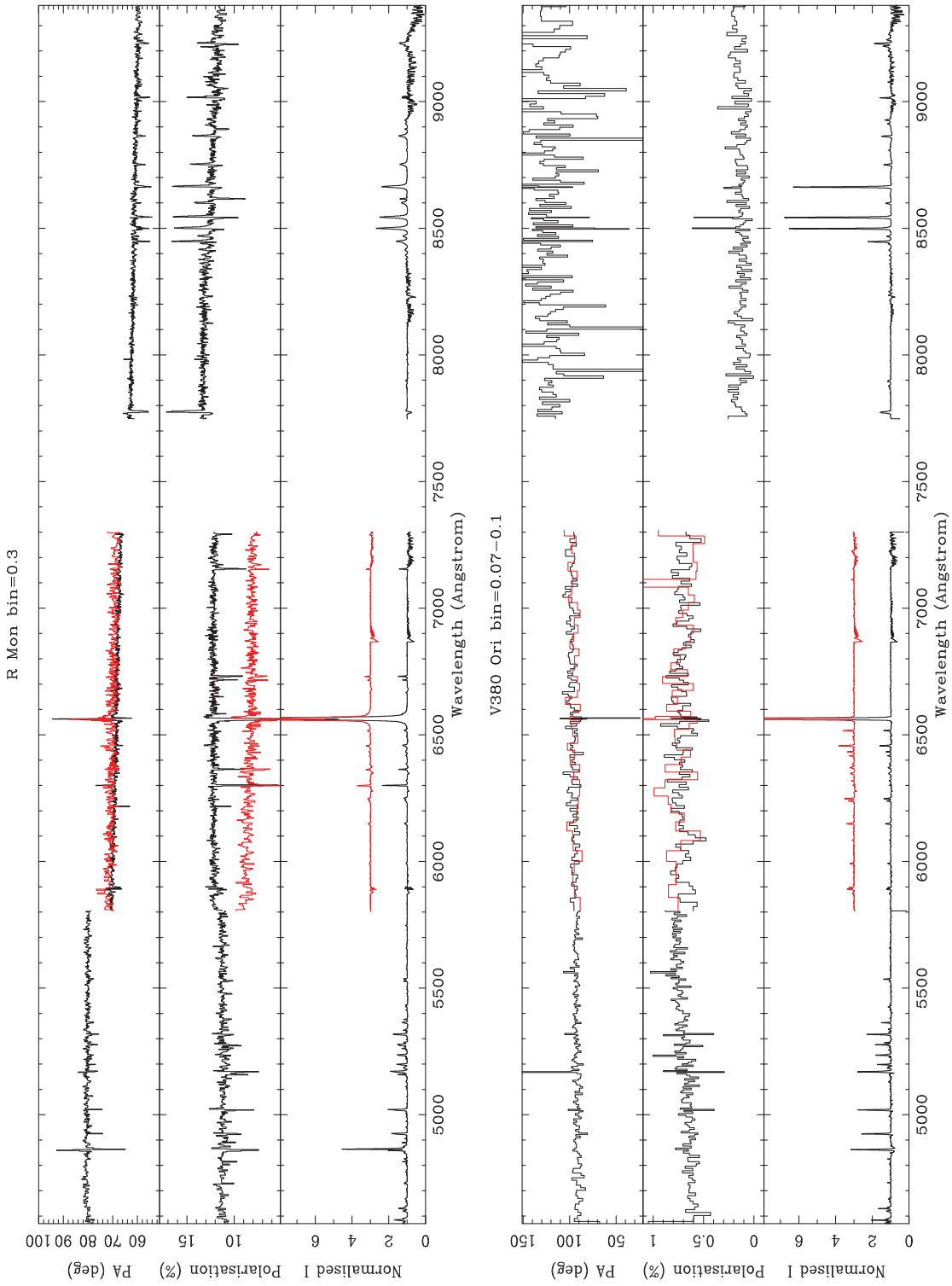

Figure A1 – *continued*

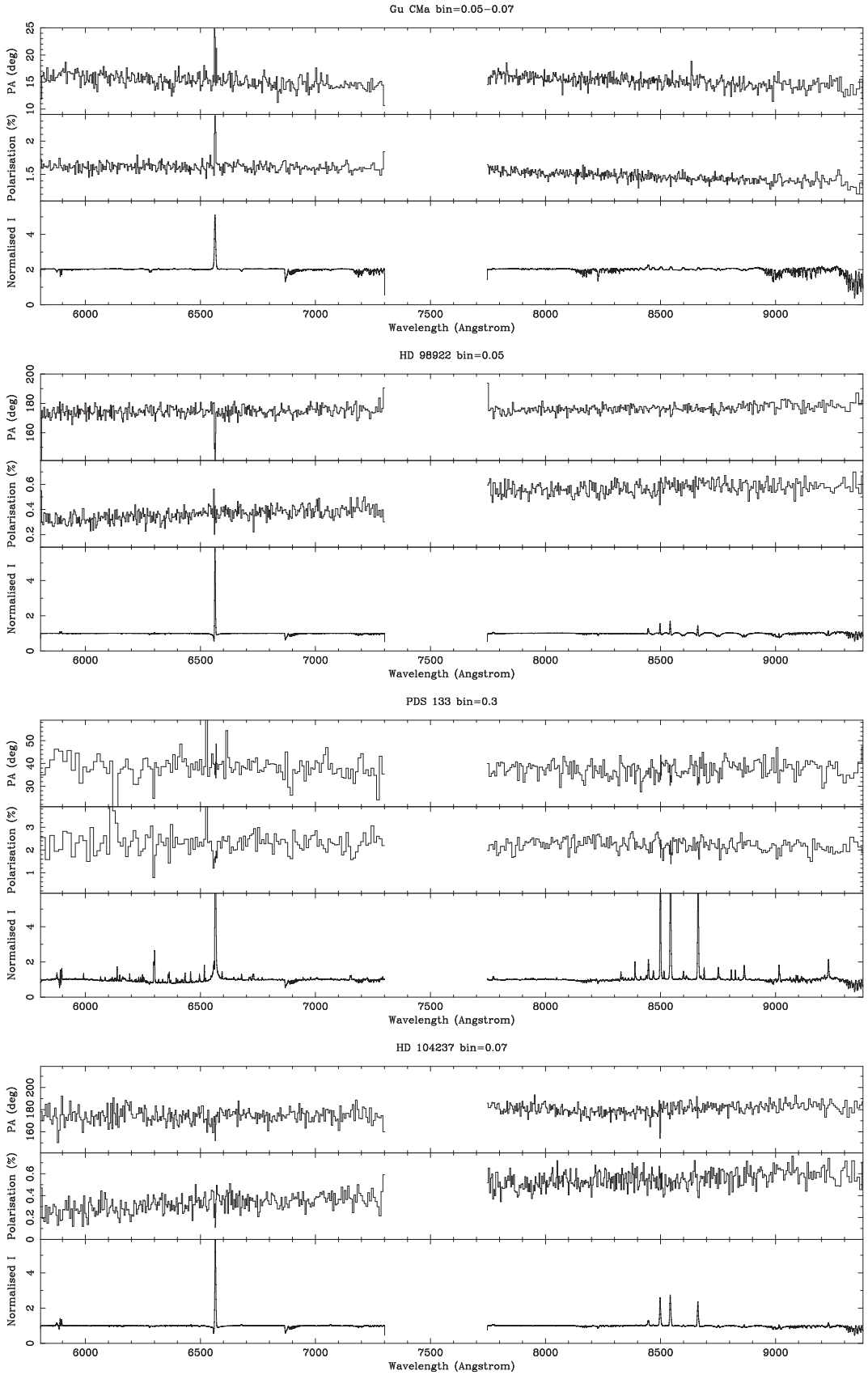

Figure A1 – *continued*

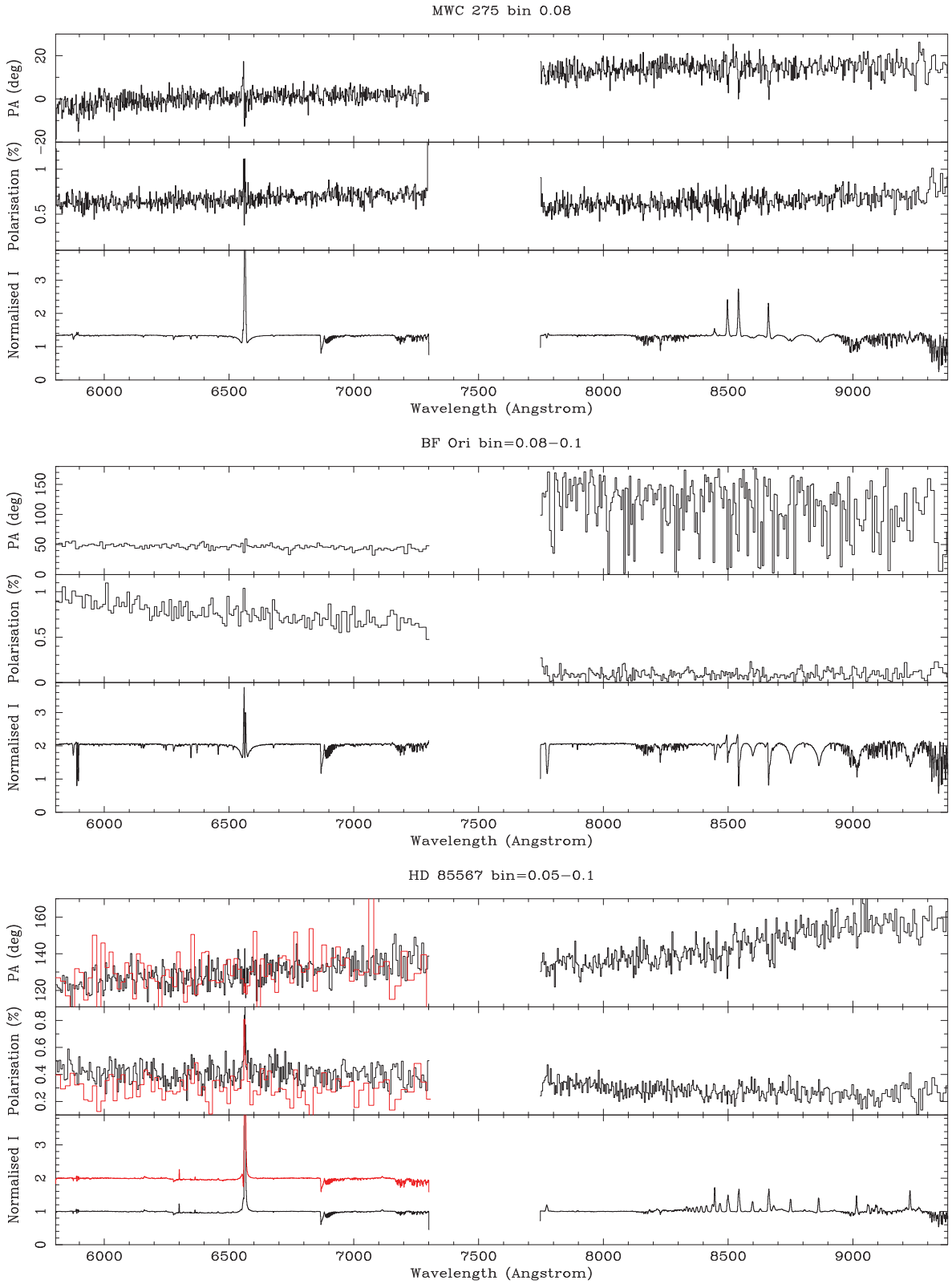

Figure A1 – *continued*

This paper has been typeset from a TEX/LATEX file prepared by the author.